Septate junctions regulate gut homeostasis through regulation of stem cell proliferation and enterocyte behavior in *Drosophila*

Yasushi Izumi[1,2], Kyoko Furuse[1], and Mikio Furuse[1,2]

[1]Division of Cell Structure, National Institute for Physiological Sciences, Okazaki, Japan

[2]Department of Physiological Sciences, SOKENDAI, Okazaki, Japan

Address correspondence and proofs to:

Yasushi Izumi, PhD, Division of Cell Structure, National Institute for Physiological Sciences, 5-1 Higashiyama, Myodaiji, Okazaki 444-8787, Japan

Tel: +81-564-59-5279; Fax: +81-564-59-5275; E-mail: yizumi@nips.ac.jp

Running title: Septate junctions and gut homeostasis

Keywords: *Drosophila*, midgut, smooth septate junction, epithelial cell, intestinal stem cell, tissue homeostasis

19 **Summary statement:** Depletion of smooth septate junction-associated proteins from
20 enterocytes in the *Drosophila* adult midgut results in intestinal hypertrophy
21 accompanied by accumulation of morphologically aberrant enterocytes and increased
22 stem cell proliferation.

23

24 **Abstract**

25 Smooth septate junctions (sSJs) contribute to the epithelial barrier, which restricts
26 leakage of solutes through the paracellular route of epithelial cells in the *Drosophila*
27 midgut. We previously identified three sSJ-associated membrane proteins, Ssk, Mesh,
28 and Tsp2A, and showed that these proteins were required for sSJ formation and
29 intestinal barrier function in the larval midgut. Here, we investigated the roles of sSJs in
30 the *Drosophila* adult midgut. Depletion of any of the sSJ-proteins from enterocytes
31 resulted in remarkably shortened lifespan and intestinal barrier dysfunction in flies.
32 Interestingly, the sSJ protein-deficient flies showed intestinal hypertrophy accompanied
33 by accumulation of morphologically abnormal enterocytes. The phenotype was
34 associated with increased stem cell proliferation and activation of the MAP kinase and
35 Jak-Stat pathways in stem cells. Loss of cytokines Unpaired2 and Unpaired3, which are
36 involved in Jak-Stat pathway activation, suppressed the intestinal hypertrophy, but not
37 the increased stem cell proliferation, in flies lacking Mesh. The present findings suggest
38 that SJs play a crucial role in maintaining tissue homeostasis through regulation of stem
39 cell proliferation and enterocyte behavior in the *Drosophila* adult midgut.

40

Introduction

The intestinal epithelium serves as a physical barrier that prevents infiltration of food-derived harmful substances, microbial contaminants, and digestive enzymes into the body. To constitute an effective intestinal barrier, specialized cell-cell junctions, namely occluding junctions, play a crucial role in regulating free diffusion of solutes through the paracellular route. Septate junctions (SJs) are occluding junctions in invertebrates and act as the functional counterparts of vertebrate tight junctions (Anderson and Van Itallie, 2009, Furuse and Tsukita, 2006, Lane, 1994, Tepass and Hartenstein, 1994). In arthropods, morphological variation of SJs has been observed among different types of epithelia (Lane, 1994, Tepass and Hartenstein, 1994). Most ectodermally-derived epithelia and the perineural sheath have pleated SJs (pSJs), while endodermally-derived epithelia, including the midgut, have smooth SJs (sSJs) (Lane, 1994, Tepass and Hartenstein, 1994). Genetic and molecular analyses in *Drosophila* have revealed a number of molecular components and functional properties of pSJs (Tepass et al., 2001, Wu and Beitel, 2004, Banerjee et al., 2006, Izumi and Furuse, 2014). In contrast, few studies have been carried out on sSJs, and their physiological role is not well understood. Recently, we identified three sSJ-specific membrane proteins: Ssk, Mesh, and Tsp2A. Ssk is a four transmembrane domain-containing protein (Yanagihashi et al., 2012). Mesh is a single-pass membrane protein containing a large extracellular region (Izumi et al., 2012). Tsp2A belongs to the tetraspanin family (Izumi et al., 2016). Zygotic loss of any of these proteins results in embryonic lethality just before hatching or at the 1st instar larva stage with impairment of sSJ formation as

well as epithelial barrier function, suggesting critical roles of sSJs (Yanagihashi et al., 2012, Izumi et al., 2012, Izumi et al., 2016, Izumi and Furuse, 2014, Furuse and Izumi, 2017).

The *Drosophila* adult midgut epithelium is composed of absorptive enterocytes (ECs), secretory enteroendocrine cells (EEs), intestinal stem cells (ISCs), EC progenitors (enteroblasts: EBs), and EE progenitors (enteroendocrine mother cells: EMCs) (Micchelli and Perrimon, 2006, Ohlstein and Spradling, 2006, Guo and Ohlstein, 2015). The sSJs are formed between adjacent ECs and between ECs and EEs (Resnik-Docampo et al., 2017). ECs and EEs are continuously renewed by proliferation and differentiation of the ISC lineage through the production of intermediate differentiating cells, EBs and EMCs. This renewal of adult midgut epithelial cells is critical for maintenance of homeostasis in the adult midgut. Recent studies have suggested that sSJs influence proliferation and differentiation of the ISC lineage in the adult midgut. Experimental suppression of Gliotactin, a tricellular junction-associated protein, in ECs led to epithelial barrier dysfunction, increased ISC proliferation, and blockade of EC differentiation in young flies (Resnik-Docampo et al., 2017). Moreover, loss of *mesh* and *Tsp2A* in clones caused defects in polarization and integration of ECs in the adult midgut (Chen et al., 2018). Thus, it will be interesting to examine the role of sSJs in the adult midgut in terms of the regulation of ISC proliferation and tissue homeostasis by genetic ablation of the sSJ-protein genes throughout ECs.

Here, we describe that depletion of the sSJ-proteins Ssk, Mesh, and Tsp2A from ECs causes remarkably reduced lifespan and midgut barrier dysfunction in flies.

The sSJ protein-deficient flies show intestinal hypertrophy accompanied by accumulation of morphologically aberrant ECs and increased stem cell proliferation. Interestingly, we show that the interleukin-6-like cytokines Unpaired2 and/or Unpaired3 are involved in this intestinal hypertrophy. We conclude that sSJs are crucial for the regulation of stem cell proliferation and EC behavior in the *Drosophila* adult midgut.

Results

Depletion of sSJ-proteins from ECs in adult flies results in shortened lifespan and midgut barrier dysfunction

To investigate the effect of sSJ-protein depletion on the *Drosophila* adult midgut, UAS-RNAi lines for sSJ-proteins were expressed in ECs using a *Myo1A*-Gal4 driver, combined with a temporal and regional gene expression targeting (TARGET) system (Zeng et al., 2010). The UAS-RNAi lines used for the sSJ-proteins were UAS-*ssk*-RNAi, *mesh*-RNAi (15074R-1), and *Tsp2A*-RNAi (11415R-2), which were confirmed to effectively reduce the expression of their respective sSJ-proteins (Yanagihashi et al., 2012, Izumi et al., 2012, Izumi et al., 2016). *Myo1A*-Gal4 tubGal80^{ts} UAS-*CD8-GFP* and UAS-*ssk*-RNAi, *mesh*-RNAi, or *Tsp2A*-RNAi (*Myo1A*^{ts}> *ssk*-RNAi, *mesh*-RNAi, or *Tsp2A*-RNAi) flies were raised to adults at 18°C and then shifted to 29°C to express each UAS-driven transgene. Almost all flies expressing the RNAis targeting the sSJ-protein transcripts (hereafter referred to as sSJp-RNAis) died within 10 days after transgene induction, while more than 95% of control flies (*Myo1A*^{ts}> *CD8-GFP*) survived until 15 days after induction (Fig. 1A).

Thus, reduced expression of sSJ-proteins in ECs results in remarkably shortened lifespan in adult flies. Next, we examined whether the barrier function of the midgut was disrupted in sSJp-RNAis flies. According to the method of a barrier integrity assay/Smurf assay method (Rera et al., 2011, Rera et al., 2012), flies were fed a non-absorbable 800-Da blue food dye in sucrose solution and observed for leakage of the dye from the midgut. At 3 days after transgene induction, reduced expression of any of the sSJ-proteins in ECs led to a significant increase in flies with blue dye throughout their body cavity, indicating defective midgut barrier function (Fig. 1C). Flies with midgut barrier dysfunction were further increased at 5 days after transgene induction, compared with age-matched controls (Fig. 1B, C). Thus, we confirmed that sSJ-proteins are required for the barrier function in the adult midgut, similar to the observations in the larval midgut (Yanagihashi et al., 2012, Izumi et al., 2012, Izumi et al., 2016).

Depletion of sSJ-proteins from ECs leads to intestinal hypertrophy accompanied by accumulation of morphologically aberrant ECs in the midgut

The shortened lifespan and midgut barrier dysfunction in sSJ-protein-deficient flies prompted us to examine the organization of their midgut epithelium. At 5 days after transgene induction, a typical simple epithelium in which ECs expressed CD8-GFP driven by *Myo1A*-Gal4 was observed in the control midgut (Fig. 2A, E). Intriguingly, the organization of the epithelium was severely disrupted in the sSJp-RNAis midgut: a large number of ECs failed to become integrated into the epithelium and instead accumulated throughout the midgut lumen (Fig. 2B–D). In addition, the ECs exhibited a

variety of aberrant appearances, implying a polarity defect (Fig. 2B–D). Indeed, abnormal distributions of actin and Dlg, a cell polarity protein, were observed in sSJp-RNAis ECs (Fig. 2B–D and Fig. S1). The most posterior part of the midgut had a hypertrophic phenotype: the lumen was filled with a large number of morphologically aberrant ECs and the diameter was severely expanded (Fig. 2F–I). We confirmed that expression of sSJp-RNAis in ECs led to decreased levels of the respective target proteins and mislocalization of other sSJ-proteins in the midgut (Fig. S2). Additional RNAi lines for *mesh* and *Tsp2A* showed essentially the same phenotypes (Fig. S3). Toluidine blue staining of semi-thin sections and ultrastructural analysis by transmission electron microscopy confirmed that morphologically aberrant cells were stratified in the sSJp-RNAis midgut (Fig. 2K–M, O–Q), while a monolayer of ECs with developed microvilli facing the lumen was observed in the control midgut (Fig. 2J, N). Notably, microvilli-like structures were often observed between stratified ECs in the sSJp-RNAis midgut (Fig. 2O, Q–S). Thus, depletion of any of the sSJ-proteins from ECs causes intestinal hypertrophy accompanied by dysplasia-like accumulation of ECs in the midgut lumen, suggesting that sSJs are required for homeostasis of the midgut organization.

Depletion of sSJ-proteins from ECs leads to increased ISC proliferation in the midgut

We speculated that the EC accumulation was caused by overproduction of ECs in the sSJp-RNAis midgut. Because regeneration of ECs depends on proliferation and

differentiation of the ISC linage, we examined whether proliferation of ISCs was increased in the sSJp-RNAis midgut. We stained the midgut with an antibody against phospho-histone H3 (PH3), a mitotic marker, and found that PH3-positive cells were markedly increased in the sSJp-RNAis midgut compared with the control midgut (Fig. 3A–D, M). Furthermore, immunostaining of the midgut with an antibody against Delta, an ISC marker, revealed that ISCs were increased in the sSJp-RNAis midgut compared with the control midgut (Fig. 3A–D, M). We also confirmed that PH3-positive cells were Delta-positive (Fig. 3A–D). Furthermore, the number of cells expressing Escargot (Esg)-LacZ, an ISC/EB marker, was increased in the *ssk*- or *mesh*-RNAi midgut (Fig. S4A–C). These results indicate that reduced expression of sSJ-proteins in ECs leads to increased ISC proliferation. Of note, Esg-LacZ signals were often observed in cells expressing CD8-GFP driven by *Myo1A*-GAL4 in the *ssk*- or *mesh*-RNAi midgut (Fig. S4E–F''), suggesting that sSJ-protein depletion causes mis-differentiation of the ISC linage in the midgut.

In the adult midgut, the Ras-MAP kinase and Jak-Stat signaling pathways are required for activation of ISC proliferation during the regeneration of epithelial cells (Buchon et al., 2010, Biteau and Jasper, 2011, Jiang and Edgar, 2009, Jiang et al., 2011, Osman et al., 2012, Zhou et al., 2013). Therefore, we examined whether these signaling pathways were activated in the sSJp-RNAis midgut. To monitor Ras-MAP kinase pathway activity, we examined the levels of phosphorylated ERK (dpERK) (Gabay et al., 1997). In control flies, dpERK signals were barely detectable in the midgut (Fig. 3E and Fig. S5A). In contrast, intense dpERK signals were observed in the sSJp-RNAis

midgut, not only in cells residing on the basal side of the epithelium, but also in some ECs (Fig. 3F–H and Fig. S5B–D), strongly suggesting that the Ras-MAP kinase pathway was activated in ISCs, EBs, and certain ECs. To monitor Jak-Stat pathway activity, we used a Stat92E reporter line driving expression of DGFP (*10xSTAT-DGFP*). In the control midgut, few DGFP-positive cells were observed (Fig. 3I and Fig. S5E, I), while DGFP-positive cells were markedly increased on the basal side of the epithelium throughout the sSJp-RNAis midgut (Fig. 3J–L and Fig. S5F–H, J–L). In addition, dpERK- and DGFP-positive signals were detected in Esg-LacZ-positive cells in the *mesh*-RNAi midgut (Fig. S6), indicating that the MAP kinase and Jak-Stat pathways were activated in the progenitor cells in the sSJ-disrupted midgut. Collectively, these results demonstrate that depletion of sSJ-proteins from ECs results in activation of both the Ras-MAP kinase and Jak-Stat signaling pathways in the midgut.

Simultaneous loss of *unpaired2* and *unpaired3* suppresses the abnormal accumulation of ECs in the *mesh*-deficient midgut

In ISC proliferation and EB differentiation, the Jak-Stat signaling pathway is activated by cytokines known as Unpaired (Upd) ligands (Jiang et al., 2009, Osman et al., 2012, Zhou et al., 2013). Upd2 and Upd3 were reported to contribute to increased ISC division in the midgut upon aging or exposure to stress (Osman et al., 2012). To examine whether Upd2 and Upd3 were involved in the increased ISC proliferation and abnormal accumulation of ECs observed in the sSJp-RNAis midgut, we suppressed *mesh* expression in the midgut of *upd2* and *upd3* double-mutant (*upd2,3*$^{\Delta}$) flies by

194 expression of *mesh*-RNAi. In the *mesh*-RNAi *upd2,3*$^{\Delta}$ midgut, a large number of mitotic
195 cells were still observed and showed a similar level to the *mesh*-RNAi midgut (Fig. 4B,
196 C, G), while only a few mitotic cells were detected in the control and *upd2,3*$^{\Delta}$ midgut
197 (Fig. 4A, G). Meanwhile, the expansion of the midgut observed in *mesh*-RNAi flies was
198 significantly suppressed in *mesh*-RNAi *upd2,3*$^{\Delta}$ flies. At 3 days after RNAi induction,
199 the diameter of the most posterior region of the midgut in *mesh*-RNAi *upd2,3*$^{\Delta}$ flies was
200 significantly smaller than that in *mesh*-RNAi flies and was similar to the *upd2,3*$^{\Delta}$ flies
201 and control flies (Fig. 4H). At 5 days after RNAi induction, the suppressive effect of
202 *upd2,3*$^{\Delta}$ in *mesh*-RNAi flies in the midgut diameter appeared to be more remarkable,
203 but it may include the influence of *upd2,3*$^{\Delta}$ alone on the midgut because the diameter of
204 the most posterior region of the midgut in *upd2,3*$^{\Delta}$ flies is smaller than that in control
205 flies in this condition (Fig. 4D–F, H). Accumulation of ECs was still observed in
206 *mesh*-RNAi *upd2,3*$^{\Delta}$ flies (Fig. 4F). The *upd2,3*$^{\Delta}$ flies expressing *mesh*-RNAi in ECs
207 exhibited a shortened lifespan, resembling that in *mesh*-RNAi flies (Fig. S7A). The
208 midgut barrier dysfunction seen in *mesh*-RNAi flies was also observed in *mesh*-RNAi
209 *upd2,3*$^{\Delta}$ flies (Fig. S7B), suggesting that Upd2 and Upd3 do not contribute to the loss of
210 barrier function in the midgut. Taken together, our observations suggest that induction
211 of Upd2 and/or Upd3 expression is responsible for the aberrant behavior of ECs in the
212 sSJp-RNAis midgut.
213
214 ***Tsp2A*-mutant clones induce non-cell-autonomous stem cell proliferation**

To further validate the effects of sSJ-protein depletion on the adult midgut, we generated mitotic clones that lacked *Tsp2A* and simultaneously expressed GFP in the ISC lineage using the mosaic analysis with a repressible cell marker (MARCM) system (Lee and Luo, 2001). The clone size, indicated by the number of GFP-positive cells per clone, of *Tsp2A*-mutant clones was comparable to that of control clones (Fig. 5A, B, G). However, an increased number of PH3-positive cells outside the mutant clones was observed in *Tsp2A*-mutant clones compared with control clones (Fig. 5A, B, H). These results indicate that loss of *Tsp2A* in ECs has a non-cell-autonomous effect on ISC proliferation. In addition, immunostaining with anti-Pdm1 and anti-Prospero (Pros) antibodies, which label ECs and EEs, respectively (Micchelli and Perrimon, 2006, Ohlstein and Spradling, 2006), revealed that *Tsp2A*-mutant clones contained differentiated ECs and EEs (Fig. 5C–F). These results suggest that loss of *Tsp2A* does not block differentiation of the ISC lineage.

Discussion

In the *Drosophila* midgut epithelium, the paracellular barrier is constructed by specialized cell-cell junctions known as sSJs (Tepass and Hartenstein, 1994). Our previous studies revealed that three sSJ-associated membrane proteins, Ssk, Mesh, and Tsp2A, are essential for the organization and function of sSJs (Yanagihashi et al., 2012, Izumi et al., 2012, Izumi et al., 2016). In this study, we depleted the sSJ-proteins from ECs in the *Drosophila* adult midgut and showed that they are also required for the barrier function in the adult midgut epithelium. Interestingly, the reduced expression of

sSJ-proteins in ECs led to remarkably shortened lifespan in adult flies, increased ISC proliferation, and intestinal hypertrophy accompanied by accumulation of morphologically aberrant ECs in the midgut. The intestinal hypertrophy caused by *mesh* depletion was suppressed by loss of *upd2* and *upd3* without profound suppression of ISC proliferation, recovery of the shortened lifespan, and recovery of the midgut barrier dysfunction. We also found that *Tsp2A*-mutant clones promoted ISC proliferation in a non-cell-autonomous manner. Taken together, we propose that sSJs play a crucial role in maintaining tissue homeostasis through regulation of ISC proliferation and EC behavior in the *Drosophila* adult midgut. The adult *Drosophila* intestine provides a powerful model to investigate the molecular mechanisms behind the emergence and progression intestinal metaplasia and dysplasia, which are associated with gastrointestinal carcinogenesis in mammals (Li and Jasper, 2016). Given that *Drosophila* intestinal dysplasia is associated with over-proliferation of ISCs and their abnormal differentiation, the intestinal hypertrophy observed in the present study should be categorized as a typical dysplasia in the *Drosophila* intestine.

Based on our observations, we hypothesize the following scenario for the hypertrophy generation in the sSJ-protein-deficient midgut. First, depletion of sSJ-proteins from ECs leads to disruption of sSJs in the midgut. Second, the impaired midgut barrier function caused by disruption of sSJs results in leakage of harmful substances from the intestinal lumen, thereby inducing the expression of cytokines and growth factors, such as Upd and EGF ligands, in the midgut. Alternatively, disruption of sSJs causes direct activation of a particular signaling pathway that induces expression

of cytokines and growth factors by ECs. Third, proliferation of ISCs is promoted by activation of the Jak-Stat and Ras-MAP kinase pathways. Fourth, EBs produced by the asymmetric division of ISCs differentiate into ECs with impaired sSJs in response to cytokines such as Upd2 and/or Upd3. Fifth, the ECs fail to integrate into the epithelial layer because of insufficient cell-cell adhesion caused by impaired sSJs, and thus become stratified in the midgut lumen to generate hypertrophy. Interestingly, loss of *upd2* and *upd3* suppressed the intestinal hypertrophy caused by depletion of *mesh*, but not the increased ISC proliferation. These findings imply that Upd2 and/or Upd3 preferentially promote EB differentiation rather than ISC proliferation. Considering that Upd-Jak-Stat signaling is required for both ISC proliferation and EB differentiation (Jiang et al., 2009), Upd2 and/or Upd3 may predominantly promote EB differentiation and accumulation of ECs, while other cytokines such as Upd1 and/or EGF ligands may activate ISC proliferation in the sSJ-disrupted midgut. In this study, we observed abnormal morphology and aberrant F-actin and Dlg distributions in *ssk*-, *mesh*-, and *Tsp2A*-RNAi ECs. Consistent with our results, Chen et al. (2018) recently reported that loss of *mesh* and *Tsp2A* in clones causes defects in polarization and integration of ECs in the adult midgut. In contrast, no remarkable defects in the organization and polarity of ECs were observed in the *ssk*-, *mesh*-, and *Tsp2A*-mutant midgut in first-instar larvae (Yanagihashi et al., 2012, Izumi et al., 2012, Izumi et al., 2016), suggesting that sSJ-proteins are not required for establishment of the initial epithelial apical-basal polarity. This discrepancy may be explained by the marked difference between the larval and adult midguts: ECs in the larval midgut are postmitotic, while those in the

281 adult midgut are capable of regeneration by the stem cell system (Lemaitre and
282 Miguel-Aliaga, 2013). In the sSJ protein-deficient adult midgut, activated proliferation
283 of ISCs generates excessive ECs. These ECs may lack sufficient cell-cell adhesion
284 because of impaired sSJs, fail to become integrated into the epithelial layer, and detach
285 from the basement membrane, leading to loss of normal polarity. Because sSJs seem to
286 be the sole continuous intercellular contacts between adjacent epithelial cells in the
287 midgut (Tepass and Hartenstein, 1994, Baumann, 2001), it is reasonable to speculate
288 that sSJ-disrupted ECs have reduced cell-cell adhesion ability.

289 A recent study revealed that depletion of the tricellular junction protein
290 Gliotactin from ECs leads to epithelial barrier dysfunction, increased ISC proliferation,
291 and blockade of differentiation in the midgut of young adult flies (Resnik-Docampo et
292 al., 2017). In contrast to the findings after depletion of sSJ-proteins in the present study,
293 the *gliotactin*-deficient midgut does not appear to exhibit intestinal hypertrophy
294 accompanied by accumulation of ECs throughout the midgut. Furthermore, the lifespan
295 of *gliotactin*-deficient flies is longer than that of sSJ-protein-deficient flies. The
296 difference in phenotypes between the two studies may reflect the difference in the
297 degrees of sSJ deficiency: disruption of entire bicellular sSJs or tricellular sSJs only.
298 Aging was also reported to be correlated with barrier dysfunction, increased ISC
299 proliferation, and accumulation of aberrant cells in the adult midgut (Biteau et al., 2008,
300 Rera et al., 2012). The hypertrophy formation in the sSJ-disrupted midgut accompanied
301 by increased ISC proliferation and accumulation of aberrant ECs raise the possibility

302 that disruption of sSJs is the primary cause of the alterations in the midgut epithelium
303 with aging.

304 During the preparation of our manuscript, two groups published interesting
305 phenotypes of the sSJ-protein-deficient adult midgut in *Drosophila* that are highly
306 related to the present study. Salazar et al. (2018) reported that reduced expression of *ssk*
307 in ECs leads to gut barrier dysfunction, altered gut morphology, increased stem cell
308 proliferation, dysbiosis, and reduced lifespan. They also showed that up-regulation of
309 Ssk in the midgut protects flies against microbial translocation, limits dysbiosis, and
310 prolongs lifespan. Meanwhile, Xu et al. (2018) reported that depletion of *Tsp2A* from
311 ISCs/EBs causes accumulation of ISCs/EBs and a swollen midgut with multilayered
312 epithelium, similar to our observations. They also showed that knockdown of *ssk* and
313 *mesh* in ISCs/EBs results in accumulation of ISCs/EBs. Importantly, they demonstrated
314 that *Tsp2A* depletion from ISCs/EBs causes excessive aPKC-Yki-JAK-Stat activity and
315 leads to increased stem cell proliferation in the midgut. They further showed that Tsp2A
316 is involved in endocytic degradation of aPKC, which antagonizes the Hippo pathway.
317 Their results strongly suggest that sSJs are directly involved in the regulation of
318 intracellular signaling for ISC proliferation. In their study, *Tsp2A* knockdown in
319 ISCs/EBs caused no defects in the midgut barrier function, in contrast to the present
320 study. This discrepancy may be due to differences in the GAL4 drivers used in each
321 study or the conditions for the barrier integrity assay/Smurf assay. In addition, Xu et al.
322 (2018) mentioned that MARCM clones generated from ISCs expressing *Tsp2A*-RNAi
323 grow much larger than control clones, while we found no remarkable size difference

between Tsp2A mutant clones and control clones. Such discrepancies need to be reconciled by future investigations. To further clarify the mechanistic details for the role of sSJs in stem cell proliferation, it will be interesting to analyze the effects of sSJ-protein depletion on the behavior of adult Malpighian tubules, which also have sSJs, as well as on a stem cell system (Singh et al., 2007).

In this study, we have demonstrated that sSJs play a crucial role in maintaining tissue homeostasis through regulation of ISC proliferation and EC behavior in the *Drosophila* adult midgut. Our sequential identification of the sSJ-proteins Ssk, Mesh, and Tsp2A has provided a *Drosophila* model system that can be used to elucidate the roles of the intestinal barrier function by experimental dysfunction of sSJs in the midgut. However, as described in this study, simple depletion of sSJ-proteins throughout the adult midgut causes phenotypes that are too drastic, involving not only disruption of the intestinal barrier function but also intestinal dysplasia and subsequent lethality. To investigate the systemic effects of intestinal barrier impairment throughout the life course of *Drosophila*, more modest depletion of sSJ-proteins is needed for future studies.

Material and Methods

Fly stocks

Fly stocks were reared on a standard cornmeal fly medium at 25°C. w^{1118} flies were used as wild-type flies unless otherwise specified. The other fly stocks used were: *y w*; *Myo1A*-GAL4 (#112001; Drosophila Genetic Resource Center (DGRC), Kyoto, Japan),

346 *tubP*-GAL80^{ts} (#7019; Bloomington Drosophila Stock Center (BDSC), Bloomington,
347 IN), *y w*; CD8-GFP (#108068; DGRC), *y w*; *Pin*^{Yt}/CyO; UAS-*mCD8-GFP* (#5130;
348 BDSC), *w*; *10xStat92E-DGFP*/CyO (#26199; BDSC), *w*; *10xStat92E-DGFP*/TM6C *Sb*
349 *Tb* (#26200; BDSC), *y w*; *esg-lacZ*/CyO (#108851; DGRC), FRT19A; *ry* (#106464;
350 DGRC).
351 The RNAi lines used were: *ssk*-RNAi (Yanagihashi et al., 2012), *mesh*-RNAi
352 (#12074R-1, 12074R-2; Fly Stocks of National Institute of Genetics (NIG-Fly),
353 Mishima, Japan) (Izumi et al., 2012), *Tsp2A*-RNAi (#11415R-2; NIG-Fly *Tsp2A*IR1-2)
354 (Izumi et al., 2016), *w*-RNAi (#28980; BDSC).
355 The mutant stocks used were: *Tsp2A*$^{1-2}$ (Izumi et al., 2016), *w upd2*^{Delta} *upd3*^{Delta}
356 (#55729; BDSC).
357 The following stocks were used to generate positively-marked MARCM clones:
358 *tub*^{P}-GAL80 *w* FRT19A; *Act5C*-GAL4, UAS-*GFP*/CyO (#42726; BDSC), FRT19A
359 *tub*^{P}-GAL80 hsFLP *w*; UAS-*mCD8GFP* (#108065; DGRC).
360
361 **Conditional expression of UAS transgenes (TARGET system)**
362 Flies are crossed and grown at 18°C until eclosion. Adult flies at 2–5 days after eclosion
363 were collected and transferred to 29°C for inactivation of Gal80. All analyses for these
364 experiments were performed on female flies, because their age-related gut pathology is
365 well established (Lemaitre and Miguel-Aliaga, 2013).
366
367 **MARCM clone induction**

Flies were crossed at 18°C. At 2–5 days after eclosion, adult flies were heat-shocked at 37°C for 1 h twice daily. Adult flies were transferred to fresh vials every 2–3 days and maintained at 25°C for 10 days after clone induction before being dissected.

Immunostaining

Adult flies were dissected in Hanks' Balanced Salt Solution and the midgut was fixed with 4% paraformaldehyde in PBS/0.2% Tween-20 for 30 min. The fixed specimens were washed three times with PBS/0.4% Triton X-100 and blocked with 5% skim milk in PBS/0.2% Tween-20. Thereafter, the samples were incubated with primary antibodies at 4°C overnight, washed three times with PBS/0.2% Tween-20, and incubated with secondary antibodies for 3 h. After another three washes, the samples were mounted in Fluoro-KEEPER (12593-64; Nakalai Tesque, Kyoto, Japan). Images were acquired with a confocal microscope (Model TCSSPE; Leica Microsystems, Wetzlar, Germany) using its accompanying software and HC PLAN Apochromat 20× NA 0.7 and HCX PL objective lenses (Leica Microsystems). Images were processed with Adobe Photoshop® software (Adobe Systems Incorporated, San Jose, CA).

Antibodies

The following primary antibodies were used: rabbit anti-Mesh (955-1; 1:1000) (Izumi et al., 2012); rabbit anti-Tsp2A (302AP; 1:200) (Izumi et al., 2016); rabbit anti-Ssk (6981-1; 1:1000) (Yanagihashi et al., 2012); mouse anti-Dlg (4F3; Developmental Studies Hybridoma Bank (DSHB), Iowa City, IA; 1:50); mouse anti-Delta (C594.9B;

390 DSHB; 1:20); mouse anti-Pros (MR1A; DSHB; 1:20); rabbit anti-Pdm1 (a gift from Dr.
391 Yu Cai; 1:500) (Yeo et al., 1995); rabbit anti-PH3 (06-570; Millipore, Darmstadt,
392 Germany; 1:1000); rabbit anti-dpERK (Cell Signaling, Danvers, MA; 1:500); rat
393 anti-GFP (GF090R; Nakalai Tesque; 1:1000); rabbit anti-GFP (598; MBL, Nagoya,
394 Japan; 1:1000), and mouse anti-β-galactosidase (Z3781; Promega, Madison, WI; 1:200).
395 Alexa Fluor 488-conjugated (A21206; Thermo Fisher, Waltham, MA) and Cy3- and
396 Cy5-conjugated (Jackson ImmunoResearch Laboratories, West Grove, PA) secondary
397 antibodies were used at 1:400 dilution. Actin was stained with Alexa Fluor 568
398 phalloidin (A12380; Thermo Fisher; 1:1000) or Alexa Fluor 647 phalloidin (A22287;
399 Thermo Fisher; 1:1000). Nuclei were stained with propidium iodide (Nakalai Tesque;
400 0.1 mg ml^{-1}).
401
402 **Electron microscopy and toluidine blue staining**
403 Adult control, *ssk*-, *mesh*-, and *Tsp2A*-RNAi flies at 5 days after transgene induction
404 were dissected and fixed overnight at 4°C with a mixture of 2.5% glutaraldehyde and
405 2% paraformaldehyde in 0.1 M cacodylate buffer (pH 7.4). The specimens including the
406 midgut were prepared as described previously (Izumi et al., 2012). Ultrathin sections
407 (50–100 nm) were double-stained with 4% hafnium (IV) chloride and lead citrate, and
408 observed with a JEM-1011 electron microscope (JEOL, Tokyo, Japan) at an
409 accelerating voltage of 80 kV. For toluidine blue staining, sections (0.5–1 μm) mounted
410 on glass slides were placed in 0.05% toluidine blue in distilled water for 2–30 min,

411 rinsed in water for 1 min, and allowed to air dry. The stained sections were observed
412 with an optical microscope (BX41; Olympus, Tokyo, Japan).
413
414 **Statistical analyses**
415 Statistical significance was evaluated by the Mann–Whitney *U*-test, Student's *t*-test
416 (KaleidaGraph software; Synergy Software, Reading, PA), and Fisher's exact test.
417 Values of $p<0.05$ were considered significant.
418
419 **Barrier integrity assay (Smurf assay)**
420 Flies at 2–5 days of age were placed in empty vials containing a piece of paper soaked
421 in 1% (wt/vol) Blue Dye No. 1 (Tokyo Chemical Industry, Tokyo, Japan)/5% sucrose
422 solution at 50–60 flies/vial. After 2 days at 18°C, the flies were placed in new vials
423 containing paper soaked in BlueDye/sucrose and transferred to 29°C. Loss of midgut
424 barrier function was determined when dye was observed outside the gut (Rera et al.,
425 2011, Rera et al., 2012). Flies were transferred to new vials every 2 days.
426
427 **Acknowledgments**
428 We are grateful to all members of the Furuse laboratories for helpful discussions. We
429 thank the Bloomington Drosophila Stock Center, Drosophila Genetic Resource Center
430 at Kyoto Institute of Technology, and Fly Stocks of National Institute of Genetics
431 (NIG-Fly) for fly stocks. We also thank Alison Sherwin, PhD, from Edanz Group
432 (www.edanzediting.com/ac) for editing a draft of this manuscript.

433

434 **Competing interests**

435 No competing interests declared.

436

437 **Author contributions**

438 Y.I. designed the research; Y.I. and K.F. performed the experiments; Y.I.

439 analyzed the data; Y.I. and M.F. wrote the paper.

440

441 **Funding**

442 This work was supported by a Grant-in-Aid for Scientific Research (C) (15K07048) to

443 YI from the Japan Society for the Promotion of Science.

444

445

References

Anderson, J. M. and Van Itallie, C. M. (2009). Physiology and function of the tight junction. *Cold Spring Harb Perspect Biol,* **1,** a002584.

Banerjee, S., Sousa, A. D. and Bhat, M. A. (2006). Organization and function of septate junctions: an evolutionary perspective. *Cell Biochem Biophys,* **46,** 65-77.

Baumann, O. (2001). Posterior midgut epithelial cells differ in their organization of the membrane skeleton from other drosophila epithelia. *Exp Cell Res,* **270,** 176-187.

Biteau, B., Hochmuth, C. E. and Jasper, H. (2008). JNK activity in somatic stem cells causes loss of tissue homeostasis in the aging Drosophila gut. *Cell Stem Cell,* **3,** 442-455.

Biteau, B. and Jasper, H. (2011). EGF signaling regulates the proliferation of intestinal stem cells in Drosophila. *Development,* **138,** 1045-1055.

Buchon, N., Broderick, N. A., Kuraishi, T. and Lemaitre, B. (2010). Drosophila EGFR pathway coordinates stem cell proliferation and gut remodeling following infection. *BMC Biol,* **8,** 152.

Chen, J., Sayadian, A. C., Lowe, N., Lovegrove, H. E. and St Johnston, D. (2018). An alternative mode of epithelial polarity in the Drosophila midgut. *PLoS Biol,* **16,** e3000041.

Furuse, M. and Izumi, Y. (2017). Molecular dissection of smooth septate junctions: understanding their roles in arthropod physiology. *Ann N Y Acad Sci,* **1397,** 17-24.

Furuse, M. and Tsukita, S. (2006). Claudins in occluding junctions of humans and flies. *Trends Cell Biol,* **16,** 181-188.

Gabay, L., Seger, R. and Shilo, B. Z. (1997). MAP kinase in situ activation atlas during Drosophila embryogenesis. *Development,* **124,** 3535-3541.

Guo, Z. and Ohlstein, B. (2015). Stem cell regulation. Bidirectional Notch signaling regulates Drosophila intestinal stem cell multipotency. *Science,* **350**.

Izumi, Y. and Furuse, M. (2014). Molecular organization and function of invertebrate occluding junctions. *Semin Cell Dev Biol,* **36,** 186-193.

Izumi, Y., Motoishi, M., Furuse, K. and Furuse, M. (2016). A tetraspanin regulates septate junction formation in Drosophila midgut. *J Cell Sci,* **129,** 1155-1164.

Izumi, Y., Yanagihashi, Y. and Furuse, M. (2012). A novel protein complex, Mesh-Ssk, is required for septate junction formation in the Drosophila midgut. *J Cell Sci,* **125,** 4923-4933.

Jiang, H. and Edgar, B. A. (2009). EGFR signaling regulates the proliferation of Drosophila adult midgut progenitors. *Development,* **136,** 483-493.

Jiang, H., Grenley, M. O., Bravo, M. J., Blumhagen, R. Z. and Edgar, B. A. (2011). EGFR/Ras/MAPK signaling mediates adult midgut epithelial homeostasis and regeneration in Drosophila. *Cell Stem Cell,* **8,** 84-95.

Jiang, H., Patel, P. H., Kohlmaier, A., Grenley, M. O., Mcewen, D. G. and Edgar, B. A. (2009). Cytokine/Jak/Stat signaling mediates regeneration and homeostasis in the Drosophila midgut. *Cell,* **137,** 1343-1355.

Lane, N. J., Dallai, R., Martinucci, G. and Burighel, P. (1994). Electron microscopic structure and evolution of epithelial janctions. *Molecular Mechanisms of Epithelial Cell Junctions: From Development to Disease (ed. S. Citi)***,** 23-43.

Lee, T. and Luo, L. (2001). Mosaic analysis with a repressible cell marker (MARCM) for Drosophila neural development. *Trends Neurosci,* **24,** 251-254.

Lemaitre, B. and Miguel-Aliaga, I. (2013). The digestive tract of Drosophila melanogaster. *Annu Rev Genet,* **47,** 377-404.

Li, H. and Jasper, H. (2016). Gastrointestinal stem cells in health and disease: from flies to humans. *Dis Model Mech,* **9,** 487-499.

Micchelli, C. A. and Perrimon, N. (2006). Evidence that stem cells reside in the adult Drosophila midgut epithelium. *Nature,* **439,** 475-479.

Ohlstein, B. and Spradling, A. (2006). The adult Drosophila posterior midgut is maintained by pluripotent stem cells. *Nature,* **439,** 470-474.

Osman, D., Buchon, N., Chakrabarti, S., Huang, Y. T., Su, W. C., Poidevin, M., Tsai, Y. C. and Lemaitre, B. (2012). Autocrine and paracrine unpaired signaling regulate intestinal stem cell maintenance and division. *J Cell Sci,* **125,** 5944-5949.

Rera, M., Bahadorani, S., Cho, J., Koehler, C. L., Ulgherait, M., Hur, J. H., Ansari, W. S., Lo, T., Jr., Jones, D. L. and Walker, D. W. (2011). Modulation of longevity and tissue homeostasis by the Drosophila PGC-1 homolog. *Cell Metab,* **14,** 623-634.

Rera, M., Clark, R. I. and Walker, D. W. (2012). Intestinal barrier dysfunction links metabolic and inflammatory markers of aging to death in Drosophila. *Proc Natl Acad Sci U S A,* **109,** 21528-21533.

Resnik-Docampo, M., Koehler, C. L., Clark, R. I., Schinaman, J. M., Sauer, V., Wong, D. M., Lewis, S., D'alterio, C., Walker, D. W. and Jones, D. L. (2017). Tricellular junctions regulate intestinal stem cell behaviour to maintain homeostasis.

Nat Cell Biol, **19,** 52-59.

Salazar, A. M., Resnik-Docampo, M., Ulgherait, M., Clark, R. I., Shirasu-Hiza, M., Jones, D. L. and Walker, D. W. (2018). Intestinal Snakeskin Limits Microbial Dysbiosis during Aging and Promotes Longevity. *iScience,* **9,** 229-243.

Singh, S. R., Liu, W. and Hou, S. X. (2007). The adult Drosophila malpighian tubules are maintained by multipotent stem cells. *Cell Stem Cell,* **1,** 191-203.

Tepass, U. and Hartenstein, V. (1994). The development of cellular junctions in the Drosophila embryo. *Dev Biol,* **161,** 563-596.

Tepass, U., Tanentzapf, G., Ward, R. and Fehon, R. (2001). Epithelial cell polarity and cell junctions in Drosophila. *Annu Rev Genet,* **35,** 747-784.

Wu, V. M. and Beitel, G. J. (2004). A junctional problem of apical proportions: epithelial tube-size control by septate junctions in the Drosophila tracheal system. *Current opinion in cell biology,* **16,** 493-499.

Xu, C., Tang, H. W., Hung, R. J., Hu, Y., Ni, X., Housden, B. E. and Perrimon, N. (2019). The Septate Junction Protein Tsp2A Restricts Intestinal Stem Cell Activity via Endocytic Regulation of aPKC and Hippo Signaling. *Cell Rep,* **26,** 670-688 e676.

Yanagihashi, Y., Usui, T., Izumi, Y., Yonemura, S., Sumida, M., Tsukita, S., Uemura, T. and Furuse, M. (2012). Snakeskin, a membrane protein associated with smooth septate junctions, is required for intestinal barrier function in Drosophila. *J Cell Sci,* **125,** 1980-1990.

Yeo, S. L., Lloyd, A., Kozak, K., Dinh, A., Dick, T., Yang, X., Sakonju, S. and Chia, W. (1995). On the functional overlap between two Drosophila POU homeo domain

533 genes and the cell fate specification of a CNS neural precursor. *Genes Dev,* **9,**
534 1223-1236.

535 **Zeng, X., Chauhan, C. and Hou, S. X.** (2010). Characterization of midgut stem cell-
536 and enteroblast-specific Gal4 lines in drosophila. *Genesis,* **48,** 607-611.

537 **Zhou, F., Rasmussen, A., Lee, S. and Agaisse, H.** (2013). The UPD3 cytokine couples
538 environmental challenge and intestinal stem cell division through modulation of
539 JAK/STAT signaling in the stem cell microenvironment. *Dev Biol,* **373,** 383-393.

540

Figure legends

Figure 1. Depletion of sSJ-proteins from ECs in adult flies results in shortened lifespan and midgut barrier dysfunction.

(A) Survival analysis of flies expressing *Myo1A*^{ts}-Gal4/UAS-*CD8-GFP* without (control, *n*=240) or with UAS-*ssk*-RNAi (*n*=220), UAS-*mesh*-RNAi (15074R-1) (*n*=239), or UAS-*Tsp2A*-RNAi (11415R-2) (*n*=220). The transgenes were expressed with temperature-sensitive GAL80, and thus the flies were raised at 18°C until adulthood and then moved to 29°C. Each vial contained 20 flies (10 females, 10 males). **(B, C)** Barrier integrity assays (Smurf assays). Flies expressing *Myo1A*^{ts}-Gal4/UAS-*CD8-GFP* without or with UAS-*ssk*-RNAi, UAS-*mesh*-RNAi, or UAS-*Tsp2A*-RNAi were fed blue dye in sucrose solution. (B) Typical examples of the phenotypes at 5 days after transgene induction. (C) Left to right: Control (*CD8-GFP*) (*n*=264), *ssk*-RNAi *CD8-GFP* (*n*=375), *mesh*-RNAi *CD8-GFP* (*n*=531), and *Tsp2A*-RNAi *CD8-GFP* (*n*=508) at 3 days after induction, Control (*CD8-GFP*) (*n*=232), *ssk*-RNAi *CD8-GFP* (*n*=299), *mesh*-RNAi *CD8-GFP* (*n*=384), and *Tsp2A*-RNAi *CD8-GFP* (*n*=336) at 5 days after induction. Loss of midgut barrier function was determined when dye was observed outside the midgut. Flies with reduced sSJ-protein expression show loss of barrier function compared with control flies (*CD8-GFP* flies). The *p*-values in (C) represent significant differences in pairwise post-test comparisons indicated by the corresponding bars (Fisher's exact test).

Figure 2. Depletion of sSJ-proteins from ECs leads to intestinal hypertrophy

562 **accompanied by accumulation of morphologically aberrant ECs in the midgut.**

563 **(A–H)** Confocal images of the adult midgut expressing *Myo1A*^{ts}-Gal4/UAS-*CD8-GFP*

564 without (A, E, control) or with UAS-*ssk*-RNAi (B, F), UAS-*mesh*-RNAi (C, G), or

565 UAS-*Tsp2A*-RNAi (D, H) at 5 days after induction stained for actin (red). CD8-GFP

566 driven by *Myo1A*^{ts} was expressed in the ECs of each midgut. A large number of ECs

567 with aberrant morphology have accumulated in the anterior (B–D) and posterior (F–H)

568 midgut. The most posterior region of the sSJp-RNAis midgut is severely expanded

569 (E–H). Scale bar: 50 μm.

570 **(I)** Diameter of the most posterior region of the midgut. The diameter of the midgut was

571 measured just anterior to the Malpighian tubules. Left to right: Control (*CD8-GFP*)

572 (n=19), *ssk*-RNAi *CD8-GFP* (n=24), *mesh*-RNAi *CD8-GFP* (n=19), and *Tsp2A*-RNAi

573 *CD8-GFP* (n=22) at 5 days after induction. Error bars show s.e.m. Statistical

574 significance (p<0.0001) was evaluated by Student's t-test.

575 (**J–M**) Toluidine blue staining of the adult female anterior midgut in control

576 (*CD8-GFP*) (J), *ssk*-RNAi *CD8-GFP* (K), *mesh*-RNAi *CD8-GFP* (L), and *Tsp2A*-RNAi

577 *CD8-GFP* (M) flies at 5 days after induction. Stratification of cells in the midgut lumen

578 is observed in the sSJp-RNAis midgut.

579 **(N–S)** Transmission electron microscopy of the adult female anterior midgut in control

580 (*CD8-GFP*) (N), *ssk*-RNAi *CD8-GFP* (O, R), *mesh*-RNAi *CD8-GFP* (P), and

581 *Tsp2A*-RNAi *CD8-GFP* (Q, S) flies at 5 days after induction. (R) and (S) are enlarged

582 views of the regions outlined by the black boxes in (O) and (Q), respectively.

583 Morphologically aberrant cells are stratified in the sSJp-RNAis midgut (K–M).

584 Microvilli-like structures are found between stratified ECs in the sSJp-RNAis midgut
585 (O, Q–S). Scale bars: 5 μm (N–Q); 15 μm (R, S). Mv, microvilli; VM, visceral muscles.
586
587 **Figure 3. Depletion of sSJ-proteins from ECs leads to increased ISC proliferation**
588 **in the midgut.**
589 **(A–H)** Confocal images of the adult anterior midgut expressing
590 *Myo1A*^{ts}-Gal4/UAS-*CD8-GFP* without (A, E, control) or with UAS-*ssk*-RNAi (B, F),
591 UAS-*mesh*-RNAi (C, G), or UAS-*Tsp2A*-RNAi (D, H) at 5 days after induction stained
592 for PH3 (red in A–D), Delta (blue in A–D), dpERK (blue in E–H), and DNA
593 (propidium iodide) (red in E–H). PH3-positive cells and Delta-positive cells are
594 increased in the sSJ-protein-deficient midgut compared with the control midgut (A–D).
595 Enhancement of Ras-MAPK pathway activity in the sSJ-protein-deficient midgut is
596 shown by increased expression of dpERK (E–H). Scale bar: 50 μm.
597 **(I–L)** Confocal images of the adult anterior midgut expressing
598 *Myo1A*^{ts}-Gal4/*10xSTAT-DGFP* without (I, control) or with UAS-*ssk*-RNAi (J),
599 UAS-*mesh*-RNAi (K), or UAS-*Tsp2A*-RNAi (L) at 5 days after induction stained for
600 GFP (green) and DNA (propidium iodide) (red). Enhancement of JAK-STAT pathway
601 activity in sSJ-protein deficient midgut is shown by increased expression of the
602 *10xSTAT-DGFP* reporter. Scale bar: 50 μm.
603 **(M)** Quantification of PH3-positive cells. The dot-plots show the numbers of
604 PH3-positive cells in individual midguts. Left to right: Control (*CD8-GFP*) (*n*=22),
605 *ssk*-RNAi *CD8-GFP* (*n*=28), *mesh*-RNAi *CD8-GFP* (*n*=28), and *Tsp2A*-RNAi

606 *CD8-GFP* (*n*=27) at 3 days after induction, Control (*CD8-GFP*) (*n*=16), *ssk*-RNAi
607 *CD8-GFP* (*n*=21), *mesh*-RNAi *CD8-GFP* (*n*=27), and *Tsp2A*-RNAi *CD8-GFP* (*n*=27)
608 at 5 days after induction. Bars and numbers in the graph represent the mean
609 PH3-positive cells in the fly lines. Statistical significance ($p<0.0001$) was evaluated by
610 the Mann–Whitney *U*-test.
611
612 **Figure 4. Loss of *upd2* and *upd3* suppresses abnormal accumulation of ECs in the**
613 ***mesh*-deficient midgut.**
614 **(A–C)** Confocal images of the *upd2,3*$^{\Delta}$ (A), *Myo1A*^{ts}-Gal4/UAS-*mesh*-RNAi (B), and
615 *Myo1A*^{ts}-Gal4/UAS-*mesh*-RNAi *upd2,3*$^{\Delta}$ (C) male fly anterior midgut at 5 days after
616 induction stained for PH3 (green) and DNA (propidium iodide) (red). In the
617 *mesh*-RNAi and *mesh*-RNAi *upd2,3*$^{\Delta}$ midgut, PH3-positive cells are increased
618 compared with the *upd2,3*$^{\Delta}$ midgut. Scale bar: 50 μm.
619 **(D–F)** Confocal images of the *upd2,3*$^{\Delta}$ (D), *Myo1A*^{ts}-Gal4/UAS-*mesh*-RNAi (E), and
620 *Myo1A*^{ts}-Gal4/UAS-*mesh*-RNAi *upd2,3*$^{\Delta}$ (F) male fly midgut at 5 days after induction
621 stained for actin (blue). The diameter of the most posterior region of the *mesh*-RNAi
622 midgut is severely expanded compared with the *upd2,3*$^{\Delta}$ midgut. The diameter of the
623 *mesh*-RNAi *upd2,3*$^{\Delta}$ posterior midgut is reduced compared with the *mesh*-RNAi midgut.
624 Scale bar: 50 μm.
625 **(G)** Quantification of PH3-positive cells in the *mesh*-RNAi and *mesh*-RNAi *upd2,3*$^{\Delta}$
626 male fly midgut. The dot-plots show the numbers of PH3-positive cells in individual
627 midguts. Left to right: Control (+/*mesh*-RNAi) (*n*=26), *upd2,3*$^{\Delta}$ (*n*=19), *mesh*-RNAi

(*Myo1A*^{ts}/*mesh*-RNAi) (*n*=22), and *mesh*-RNAi *upd2,3*$^{\Delta}$ (*upd2,3*$^{\Delta}$, *Myo1A*^{ts} /*mesh*-RNAi) (*n*=18) at 3 and 5 days after induction. The bars and numbers in the graph represent the mean PH3-positive cells in the fly lines. Statistical significance was evaluated by the Mann–Whitney *U*-test.

(H) Diameter of the most posterior region of Control (+/*mesh*-RNAi) (*n*=27), *upd2,3*$^{\Delta}$ (*n*=16), *mesh*-RNAi (*Myo1A*^{ts}/*mesh*-RNAi) (*n*=23), and *mesh*-RNAi *upd2,3*$^{\Delta}$(*upd2,3*$^{\Delta}$, *Myo1A*^{ts} /*mesh*-RNAi) (*n*=19) male fly midgut at 3 and 5 days after induction. The diameter of the midgut was measured just anterior to the Malpighian tubules. Error bars show s.e.m. Statistical significance was evaluated by Student's *t*-test.

Figure 5. *Tsp2A*-mutant clones induce non-cell-autonomous stem cell proliferation.

(A–F) Confocal images of the midgut from control clones (A, C, E) or *Tsp2A*$^{1-2}$ mutant clones (B, D, F) stained for GFP (green in A–F), PH3 (red in A, B), Pdm1 (red in C and D), and Pros (red in E and F). Control and *Tsp2A*$^{1-2}$ mutant clones were generated using the MARCM system and marked by GFP expression. The *Tsp2A*$^{1-2}$ mutant clones induce cell division of neighboring cells (arrows in B). In the *Tsp2A*$^{1-2}$ mutant clones, Pdm1- and Pros-positive cells are generated, similar to the control clones (arrows in C–F). Scale bar: 50 μm.

(G) Quantification of average clone size for control and *Tsp2A*$^{1-2}$ mutant clones. Error bars show s.e.m. Statistical significance was evaluated by the Mann–Whitney *U*-test. NS, not significant.

(H) Quantification of control and *Tsp2A*$^{1-2}$ mutant clones containing PH3-positive cells

650 on the inside or outside of the clones. A total of 107 control clones and 197 *Tsp2A*$^{1-2}$
651 mutant clones were counted (each clone contained >2 cells). The *p*-value represents a
652 significant difference in pairwise post-test comparisons indicated by the corresponding
653 bars (Fisher's exact test). NS, not significant.
654
655 **Figure S1. Dlg is mislocalized in sSJ-protein-deficient ECs.**
656 **(A–D')** Confocal images of the adult anterior midgut expressing
657 *Myo1A*^{ts}-Gal4/UAS-*CD8-GFP* without (A, A', control) or with UAS-*ssk*-RNAi (B, B'),
658 UAS-*mesh*-RNAi (C, C'), or UAS-*Tsp2A*-RNAi (D, D') at 5 days after induction
659 stained for Dlg (red). The images show an optical cross-section through the center of the
660 midgut. Scale bar: 20 μm.
661
662 **Figure S2. Expression of sSJp-RNAis in ECs leads to decreased levels of the**
663 **respective target proteins and mislocalization of other sSJ-proteins in the midgut.**
664 **(A–L')** Confocal images of the adult anterior midgut expressing
665 *Myo1A*^{ts}-Gal4/UAS-*CD8-GFP* without (A, A', E, E', I, I', control) or with
666 UAS-*ssk*-RNAi (B, B', F, F', J, J'), UAS-*mesh*-RNAi (C, C', G, G' K, K'), or
667 UAS-*Tsp2A*-RNAi (D, D', H, H', L, L') at 5 days after induction stained for Ssk (red in
668 A–D), Mesh (red in E–H), Tsp2A (red in I–L), and actin (blue in A'–L'). Scale bar: 50
669 μm.
670

671 **Figure S3. Expression of additional RNAi lines of *mesh* and *Tsp2A* in the adult**
672 **midgut causes increased ISC proliferation and intestinal hypertrophy.**
673 **(A–F)** Confocal images of the adult anterior (A–C) and posterior (D–F) midgut
674 expressing *Myo1A*^{ts}-Gal4/UAS-*CD8-GFP* with UAS-*white*-RNAi (JF01545) (A, D,
675 control), UAS-*mesh*-RNAi (12074R-2) (B, E), or UAS-*Tsp2A*-RNAi (*Tsp2A*IR1-2) (C,
676 F) at 5 days after induction stained for PH3 (red in A–C) and actin (red in D–F). The
677 dots in (A–C) show the outline of the midgut. Scale bar: 50 μm.
678 **(G)** Quantification of PH3-positive cells. The number of PH3-positive cells per midgut
679 was counted at 5 days after induction. The dot-plots show the numbers of PH3-positive
680 cells in individual midguts. Left to right: Control (*white*-RNAi *CD8-GFP*) (*n*=38),
681 *mesh*-RNAi *CD8-GFP* (*n*=17), and *Tsp2A*-RNAi *CD8-GFP* (*n*=15). The bars and
682 numbers in the graph represent the mean PH3-positive cells in the fly lines. Statistical
683 significance was evaluated by the Mann–Whitney *U*-test.
684 **(H)** Diameter of the most posterior region of the midgut. The diameter of the midgut
685 was measured just anterior to the Malpighian tubules at 5 days after induction. Left to
686 right: Control (*white*-RNAi *CD8-GFP*) (*n*=23), *mesh*-RNAi *CD8-GFP* (*n*=14), and
687 *Tsp2A*-RNAi *CD8-GFP* (*n*=17). Error bars show s.e.m. Statistical significance was
688 evaluated by Student's *t*-test.
689
690 **Figure S4. Depletion of *ssk* and *mesh* from ECs leads to an increase in**
691 **Esg-LacZ-positive cells.**

692 **(A–F'')** Confocal images of the adult anterior midgut expressing
693 *Myo1A*^{ts}-Gal4/UAS-*CD8-GFP/esg-lacZ* without (A, D, D', D'', control) or with
694 UAS-*ssk*-RNAi (B, E, E', E'') or UAS-*mesh*-RNAi (C, F, F', F'') at 5 days after
695 induction stained for β-galactosidase (green in A–C, red in D', D'', E', E'', F', F'').
696 The images show an optical cross-section through the center of the midgut (D–F''). The
697 arrows in D–F'' indicate CD8-GFP-driven *Myo1A*-GAL*4* and Esg-LacZ
698 double-positive cells. Scale bar: 50 μm.
699
700 **Figure S5. The Ras-MAP kinase pathway is activated in some ECs in the**
701 **sSJ-protein-deficient midgut.**
702 **(A–D)** Confocal images of the adult anterior midgut expressing
703 *Myo1A*^{ts}-Gal4/UAS-*CD8-GFP* without (A, control) or with UAS-*ssk*-RNAi (B),
704 UAS-*mesh*-RNAi (C), or UAS-*Tsp2A*-RNAi (D) at 5 days after induction stained for
705 dpERK (red). The arrows indicate CD8-GFP-driven *Myo1A*-GAL4 (green) and dpERK
706 double-positive cells. Scale bar: 50 μm.
707 **(E–L)** Confocal images of the adult anterior midgut expressing
708 *Myo1A*^{ts}-Gal4/*10xSTAT-DGFP* without (E, I, control) or with UAS-*ssk*-RNAi (F, J),
709 UAS-*mesh*-RNAi (G, K), or UAS-*Tsp2A*-RNAi (H, L) at 5 days after induction stained
710 for GFP (green in E–L), DNA (propidium iodide) (red in E–H), and actin (red in I–L).
711 (E and I), (F and J), (K and L), and (H and L) are each derived from the same sample.
712 The images show an optical cross-section through the center of the midgut (A–L). Scale
713 bar: 50 μm.

Figure S6. The Ras-MAP kinase and Jak-Stat pathways are activated in Esg-LacZ-positive cells in the *mesh*-deficient midgut.

(A–D'') Confocal images of the adult posterior midgut expressing *Myo1A*^{ts}-Gal4/UAS-*CD8-GFP*/*esg-lacZ* without (A–A'', C–C'', control) or with UAS-*mesh*-RNAi (B–B'', D–D'') at 5 days after induction stained for β-galactosidase (red in A', A'', B', B'', C', C'', D', D''), dpERK (green in A, A'', B, B''), and GFP (green in C, C'', D, D''). (A and C) and (B and D) are each derived from the same sample. Scale bar: 50 μm.

Figure S7. Depletion of *mesh* from ECs results in shortened lifespan and midgut barrier dysfunction in *upd2,3*$^{\Delta}$ mutant flies.

(A) Survival analysis of *upd2,3*$^{\Delta}$ (*n*=240), *Myo1A*^{ts}-Gal4/UAS-*mesh*-RNAi (*n*=180), and *Myo1A*^{ts}-Gal4/UAS-*mesh*-RNAi *upd2,3*$^{\Delta}$ (*n*=260) male flies. Each vial contained 20 male flies.

(B) Barrier integrity assays (Smurf assays). In these assays, *upd2,3*$^{\Delta}$ (*n*=209), *Myo1A*^{ts}-Gal4/UAS-*mesh*-RNAi (*n*=192), and *Myo1A*^{ts}-Gal4/UAS-*mesh*-RNAi *upd2,3*$^{\Delta}$ (*n*=152) male flies were fed blue dye in sucrose solution. At 5 days after induction, the phenotypes were examined. The *p*-values represent significant differences in pairwise post-test comparisons indicated by the corresponding bars (Fisher's exact test).

A

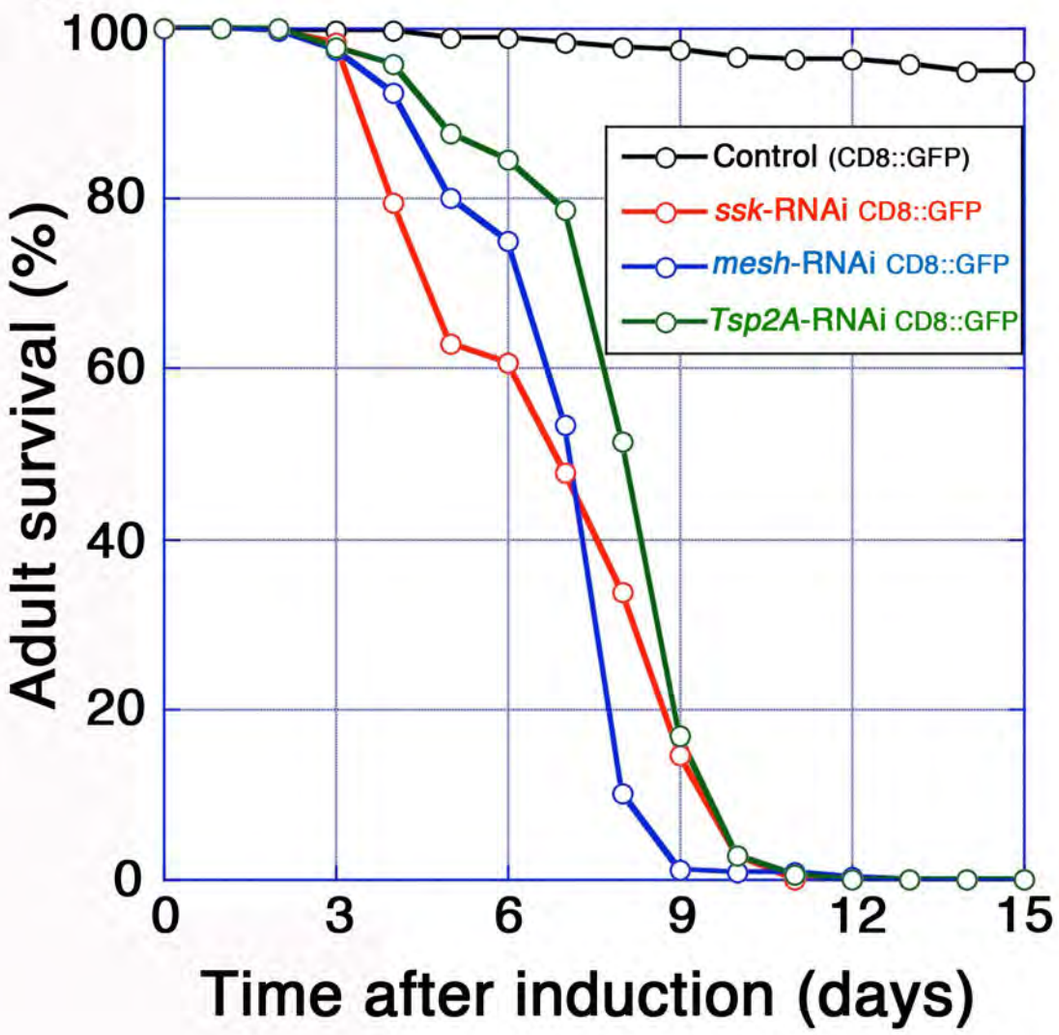

B

C

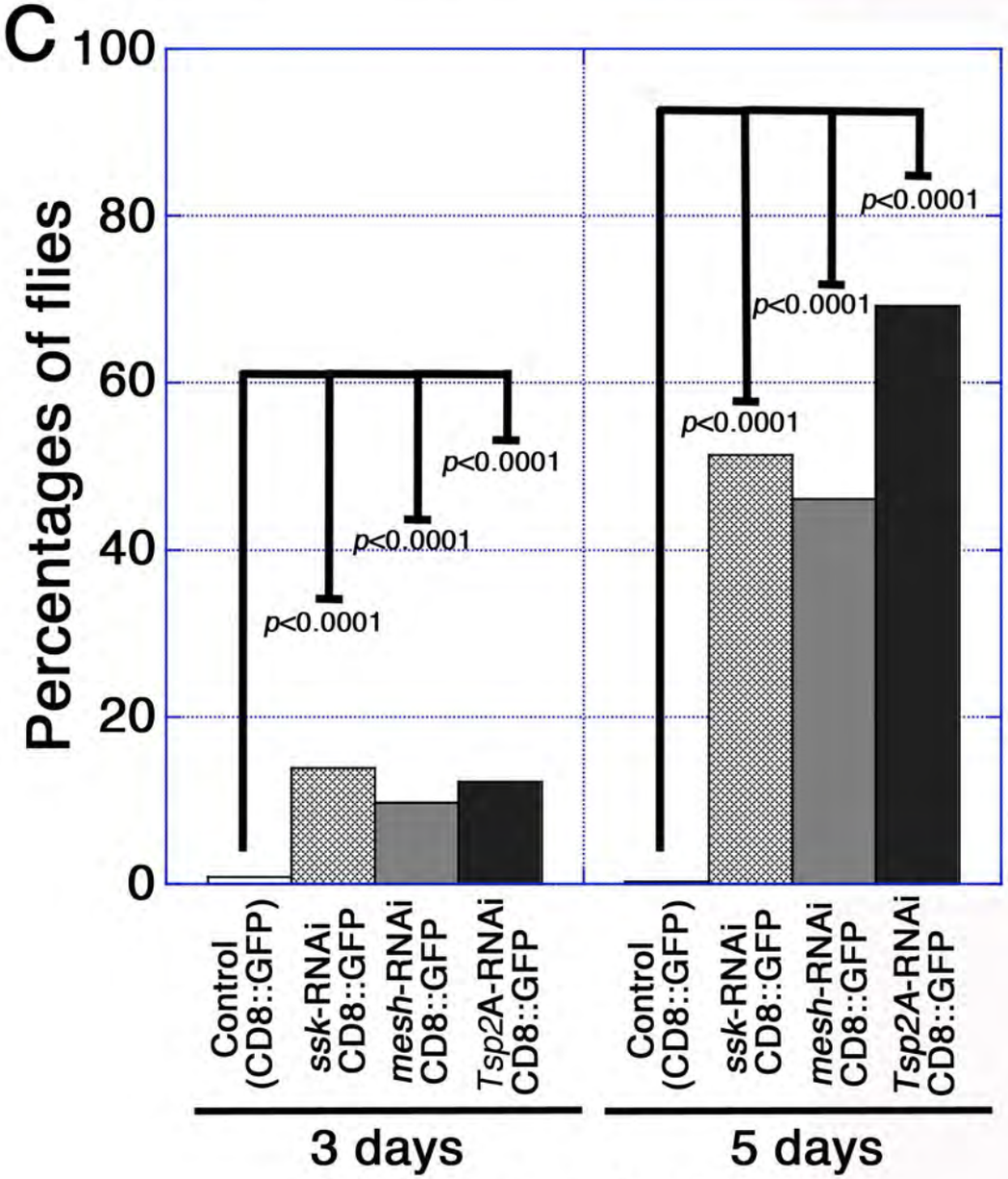

Izumi et al., Figure 1

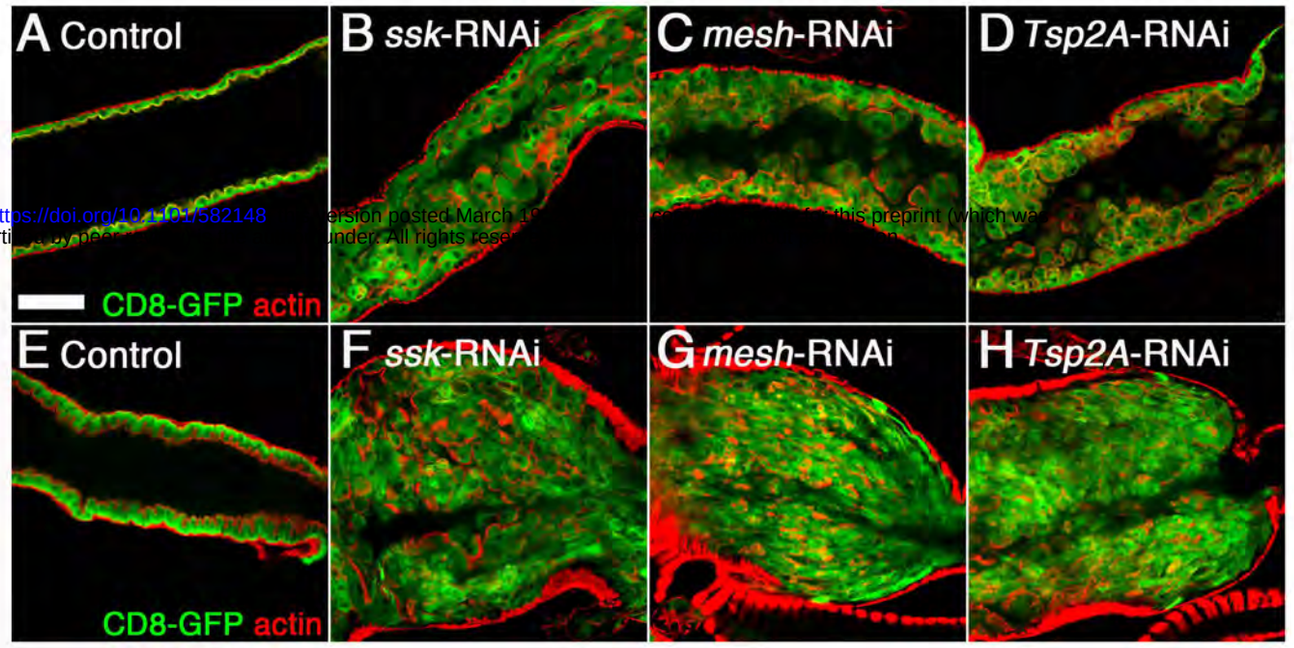

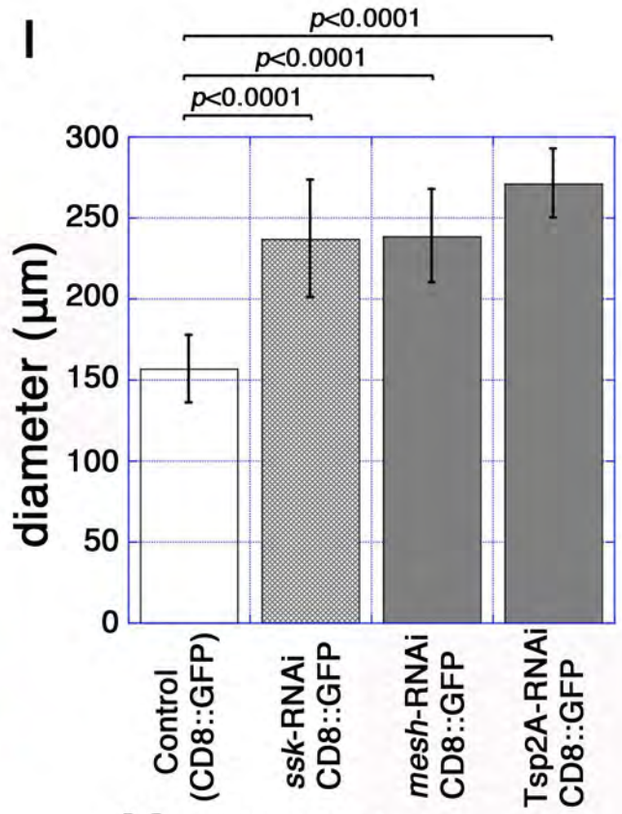

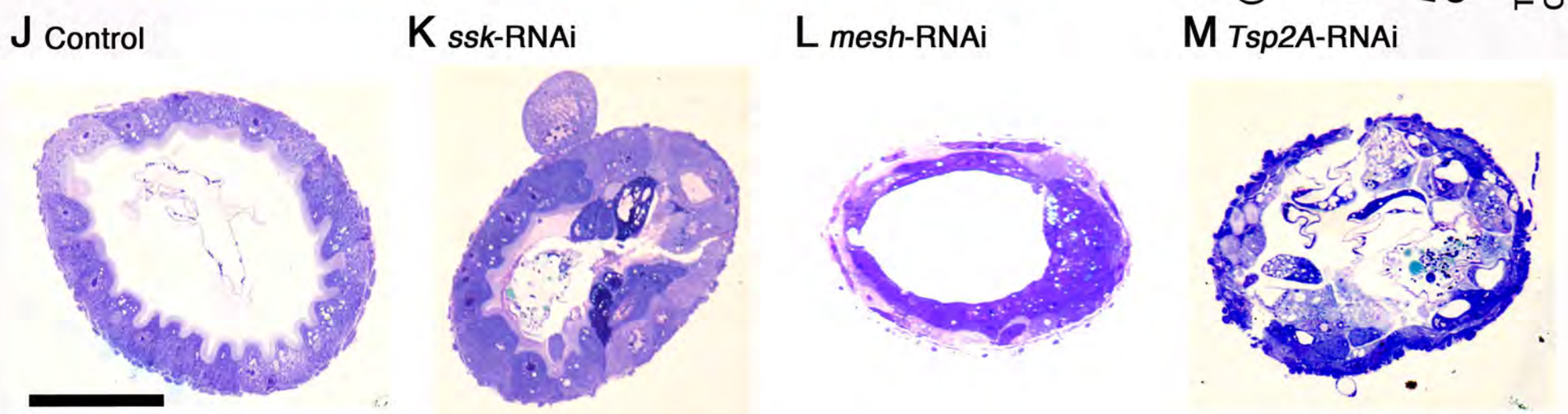

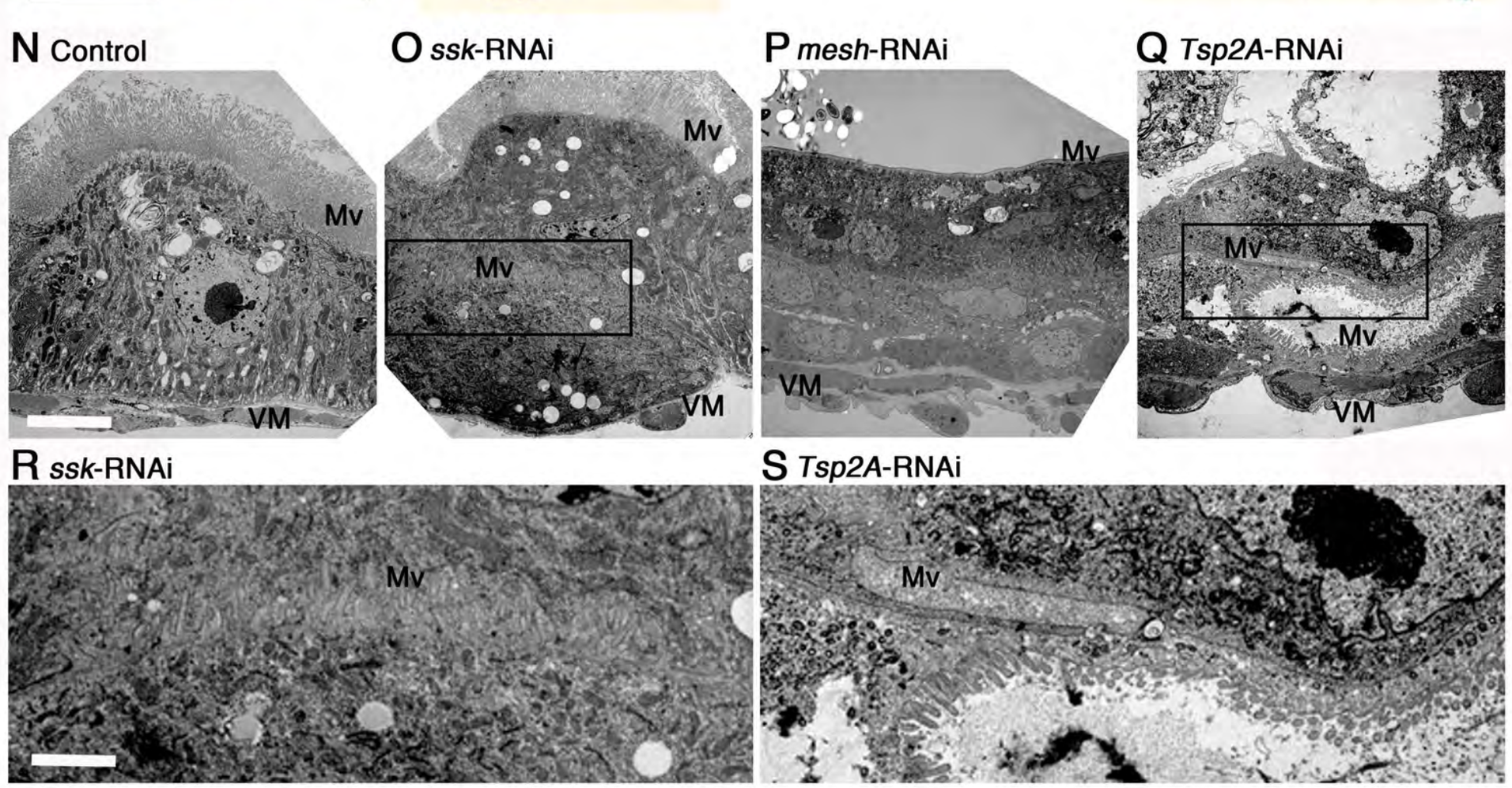

Izumi et al., Figure 2

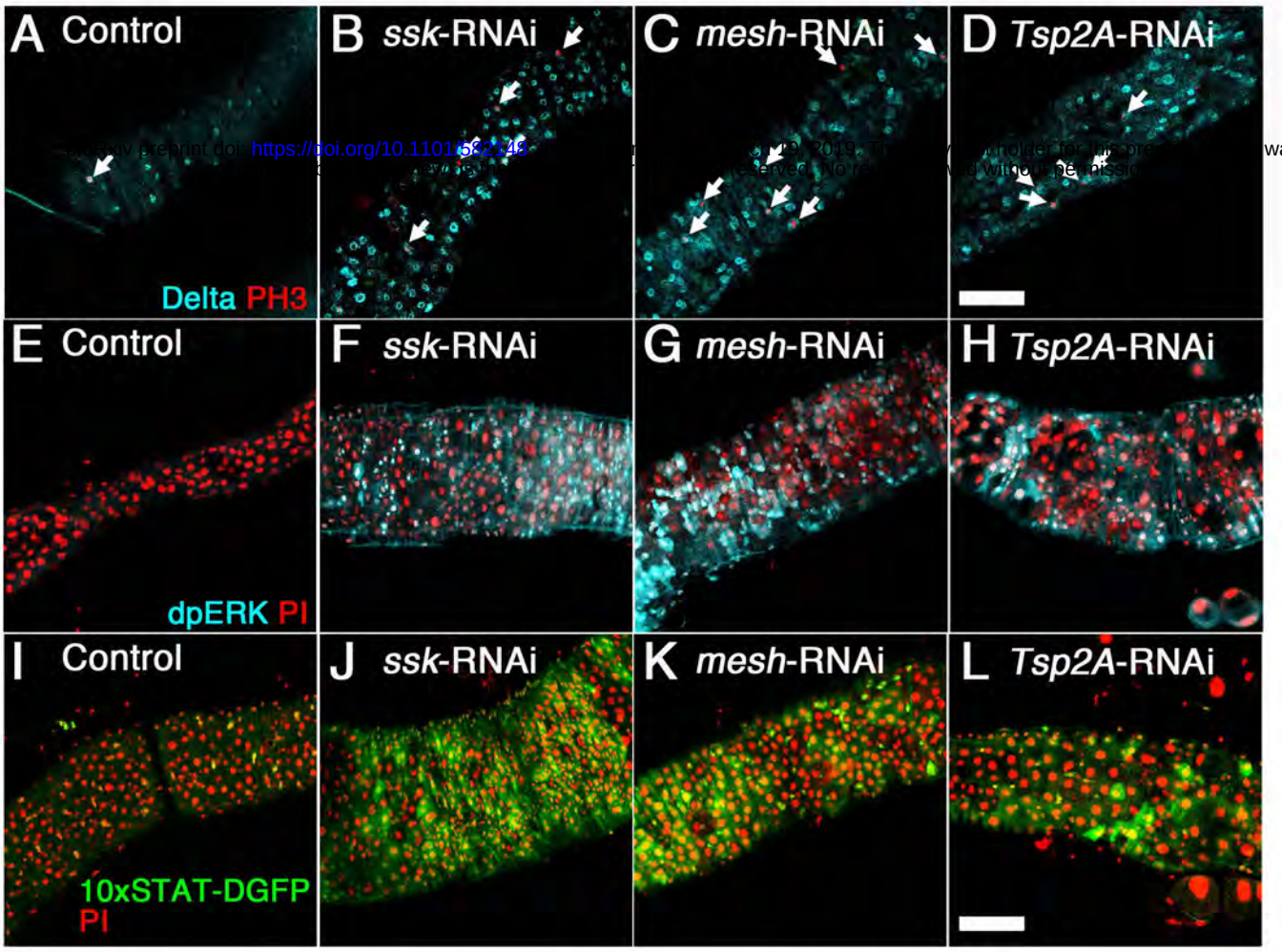

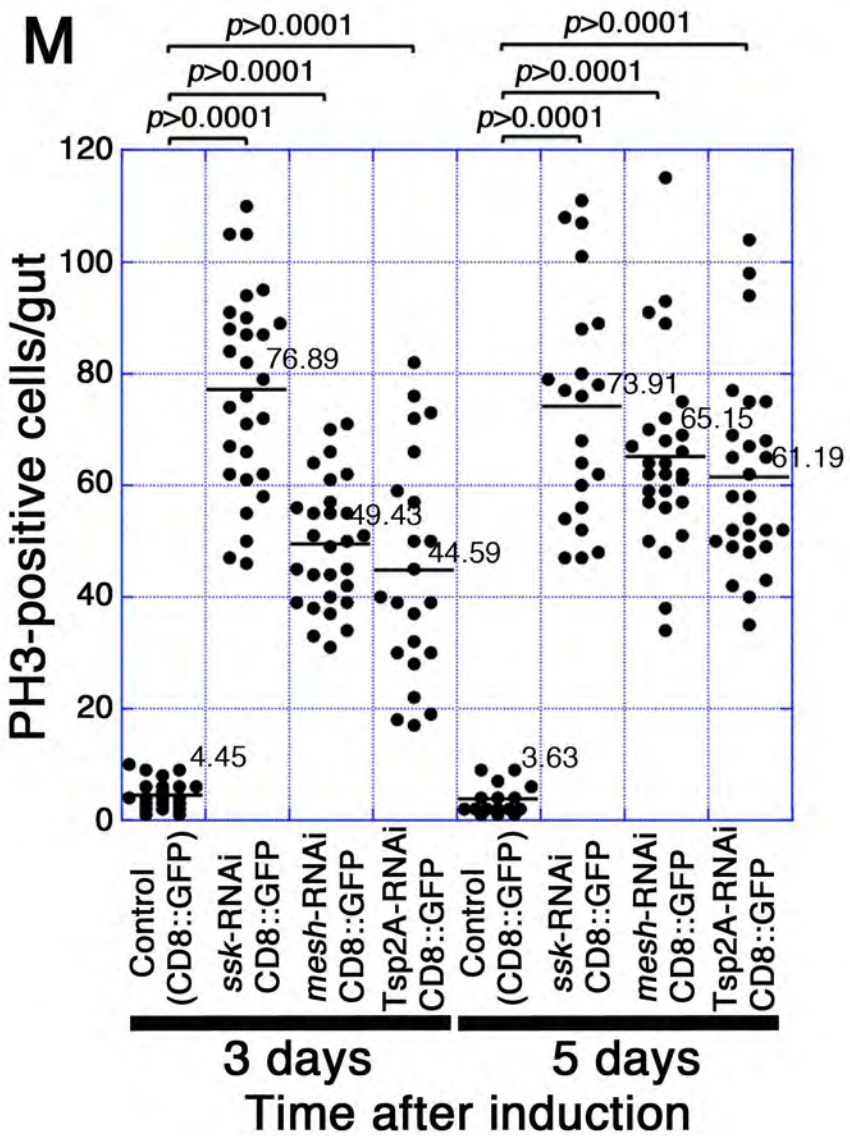

Izumi et al., Figure 3

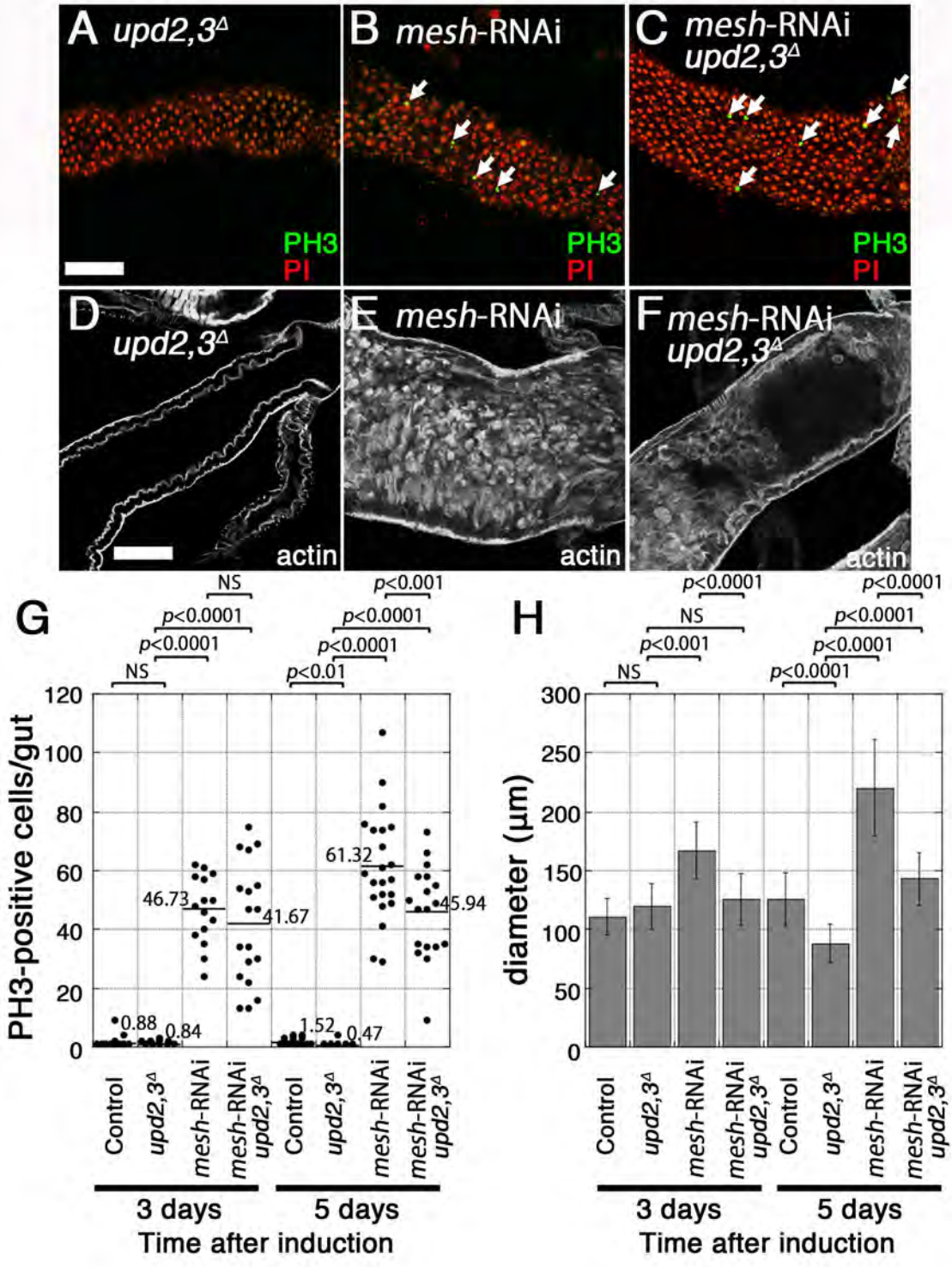

Izumi et al., Figure 4

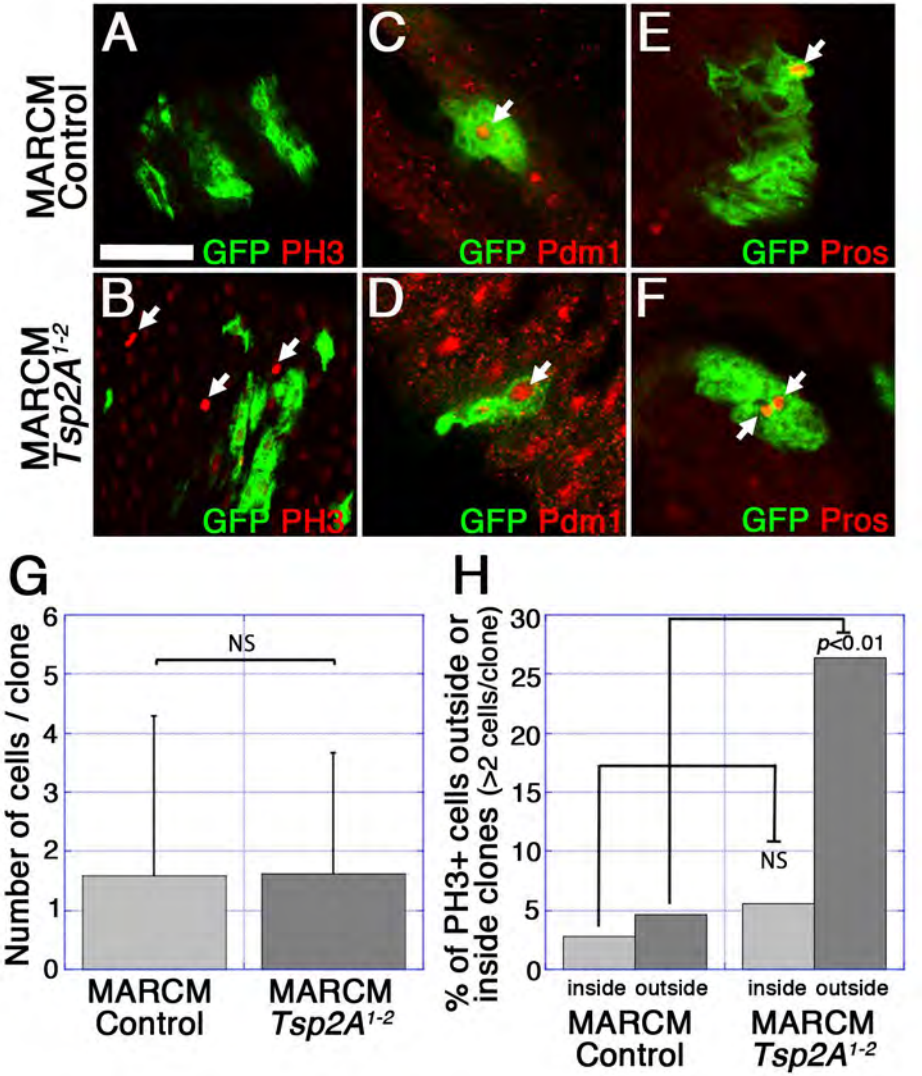

Izumi et al., Figure 5

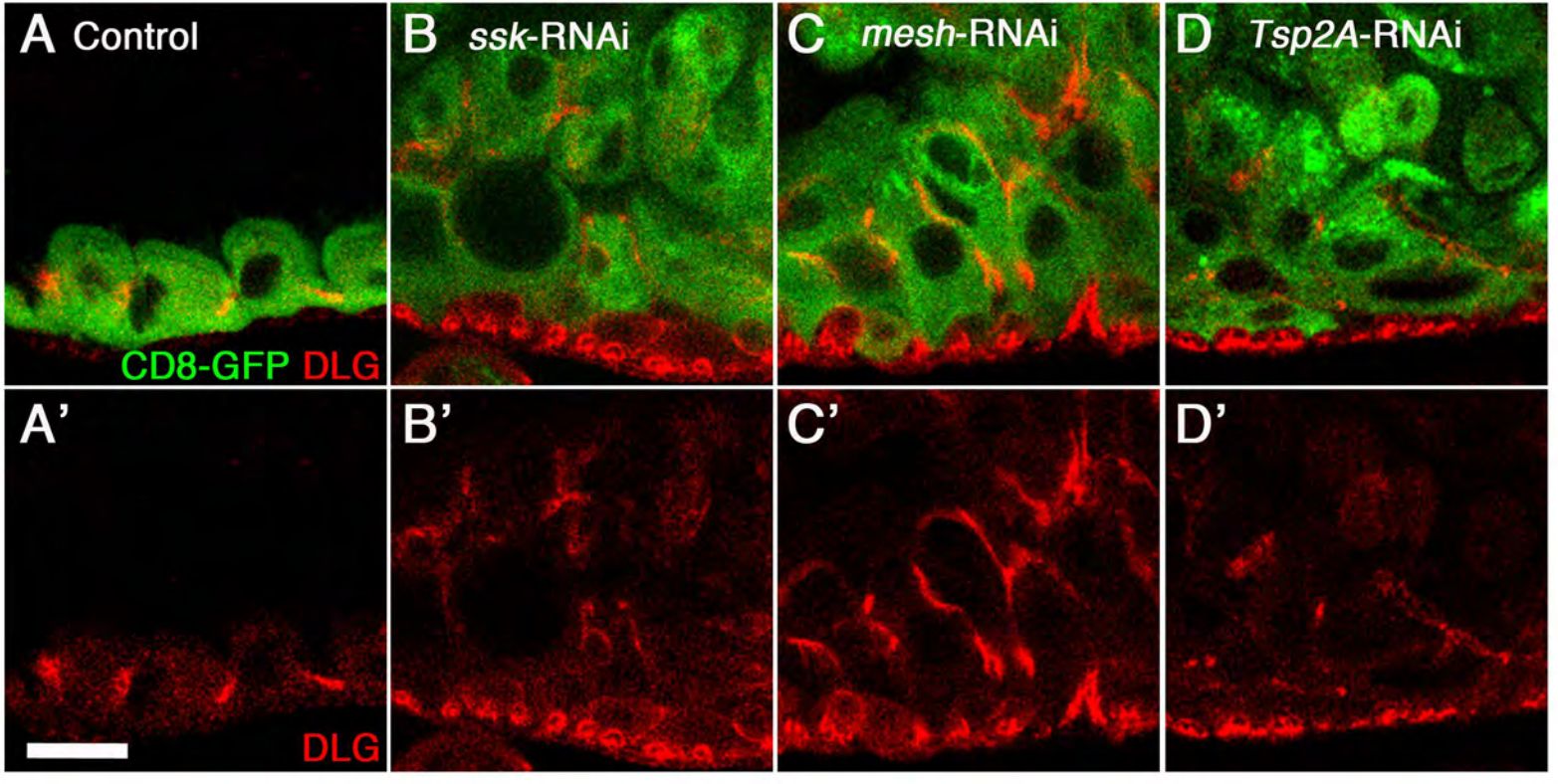

Izumi et al., Figure S1

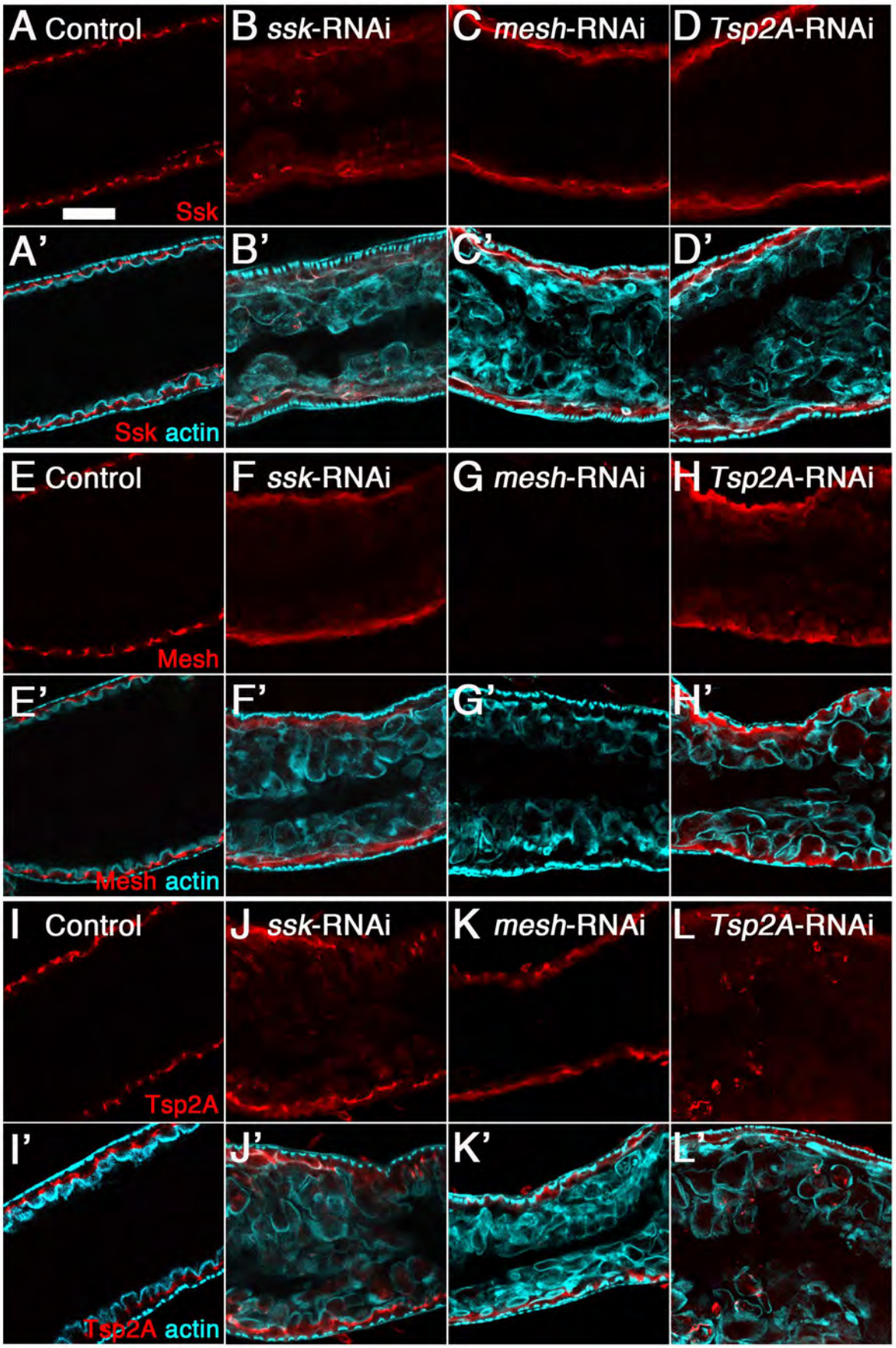

Izumi et al., Figure S2

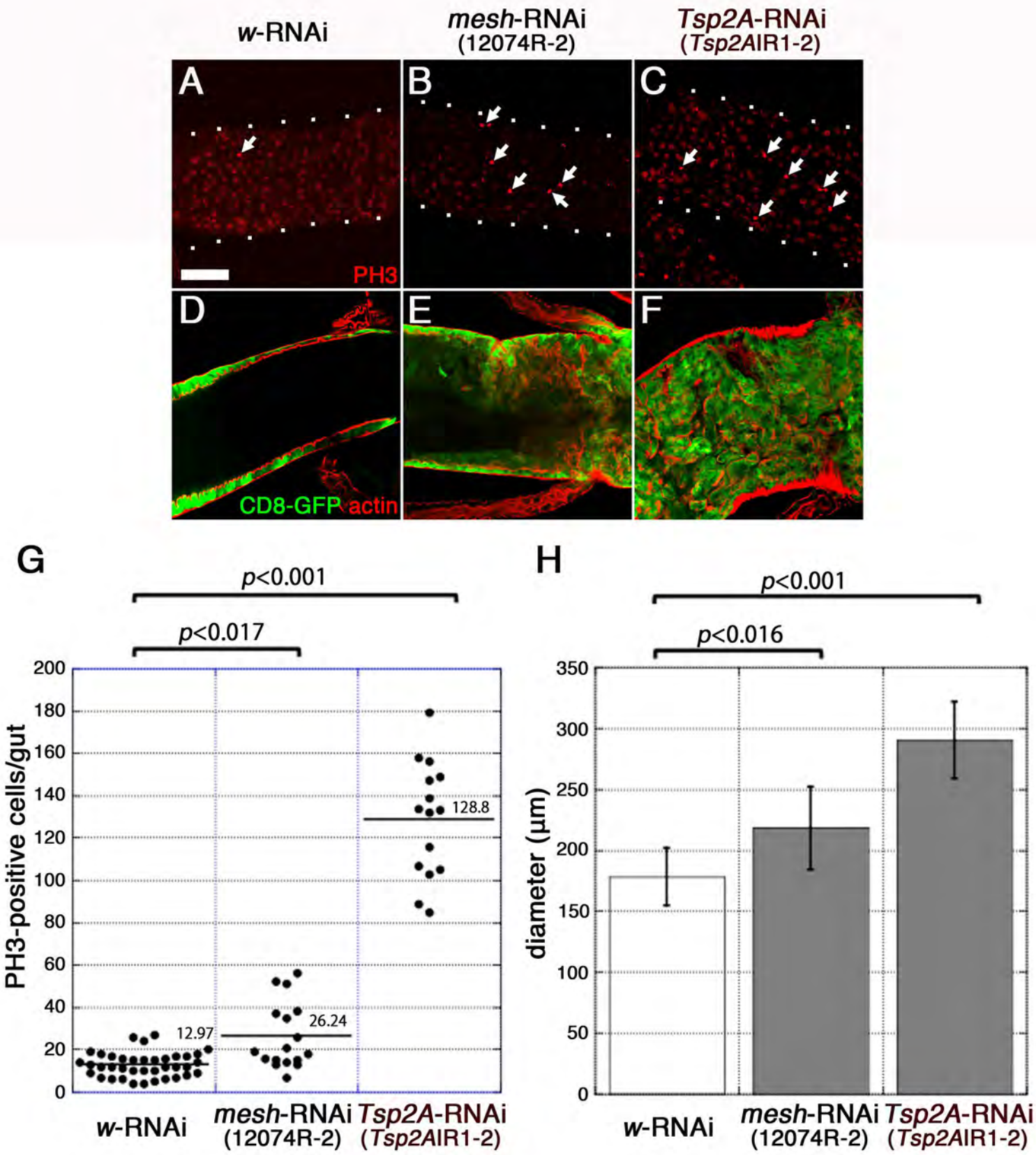

Izumi et al., Figure S3

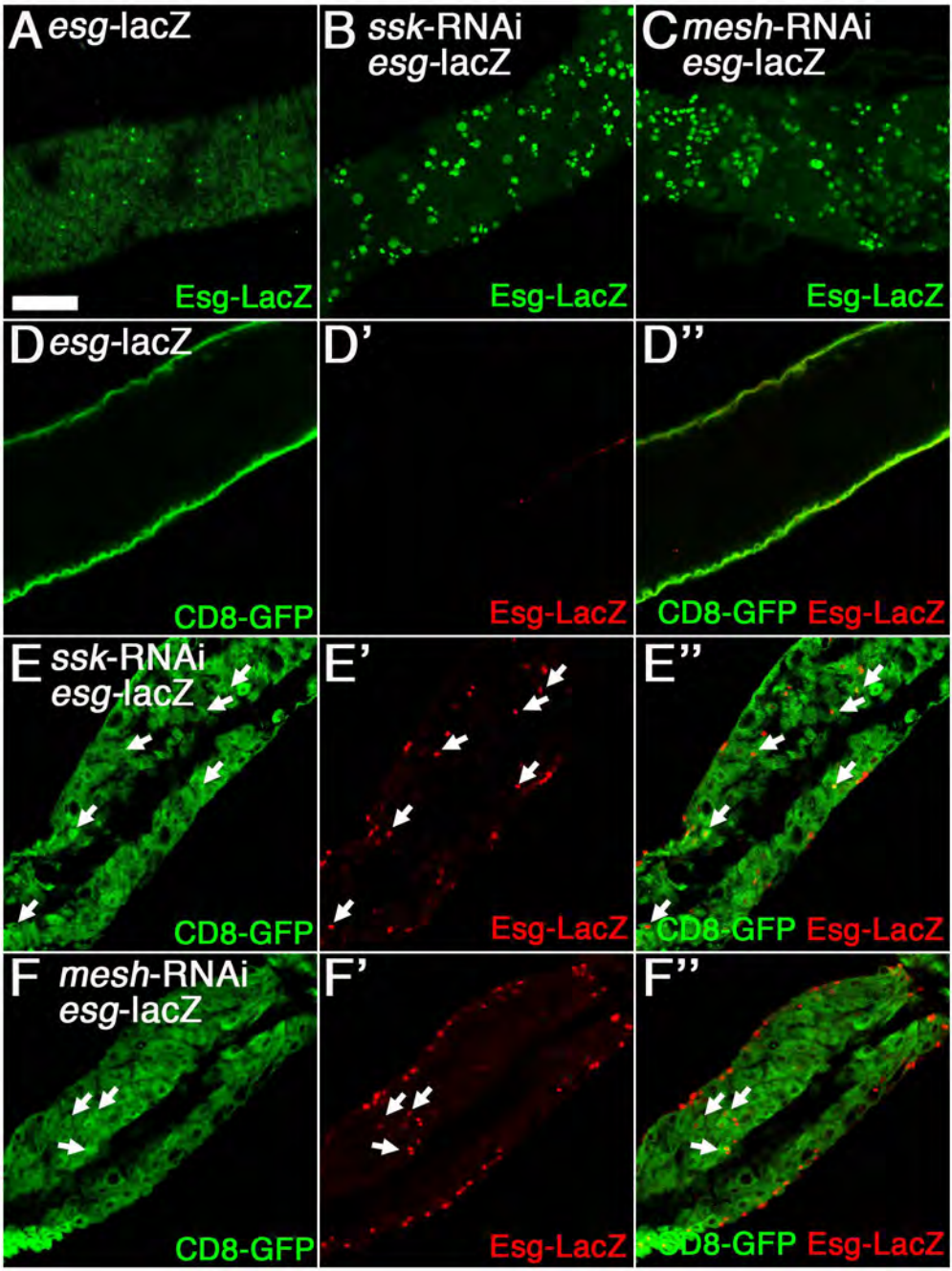

Izumi et al., Figure S4

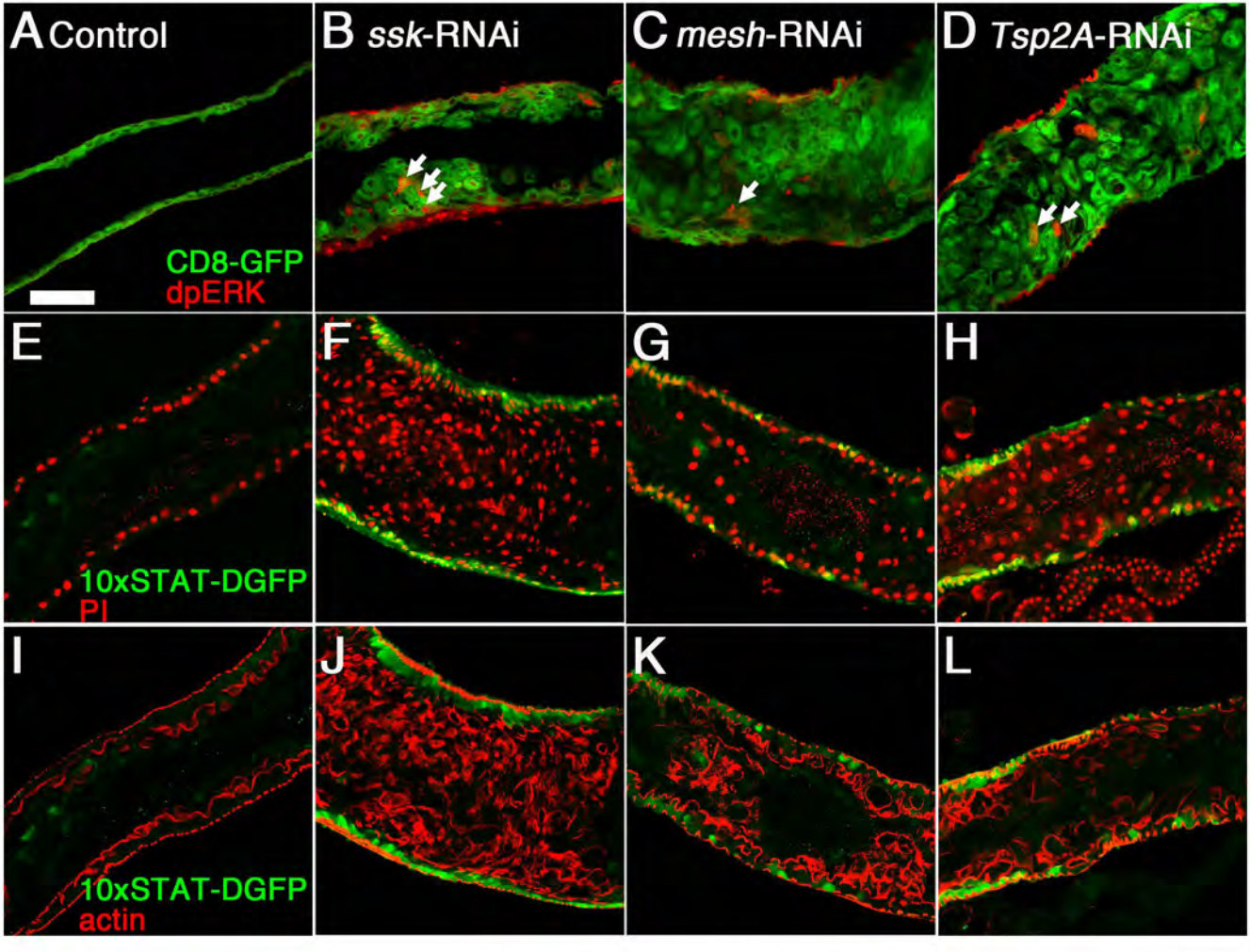

Izumi et al., Figure S5

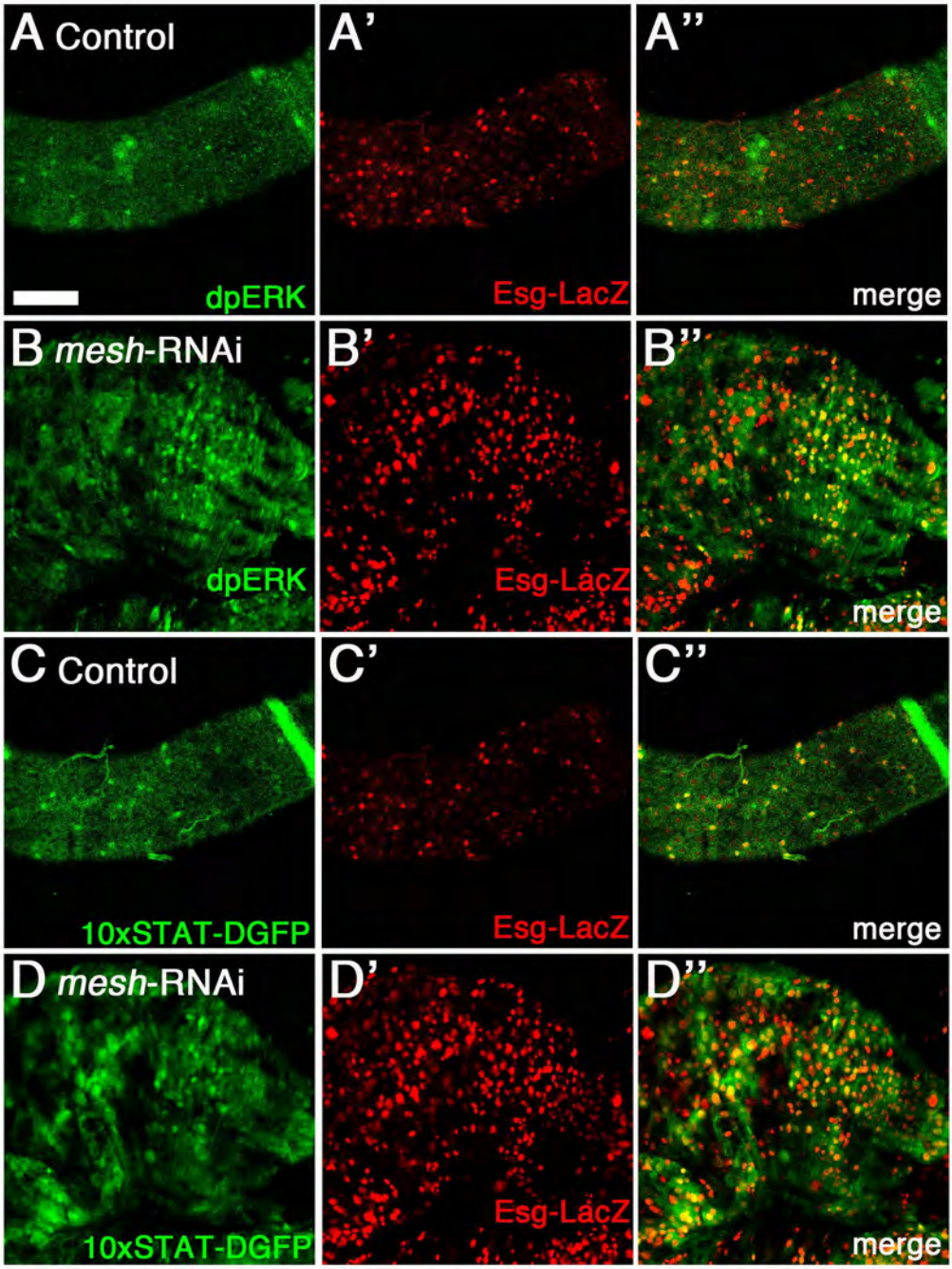

Izumi et al., Figure S6

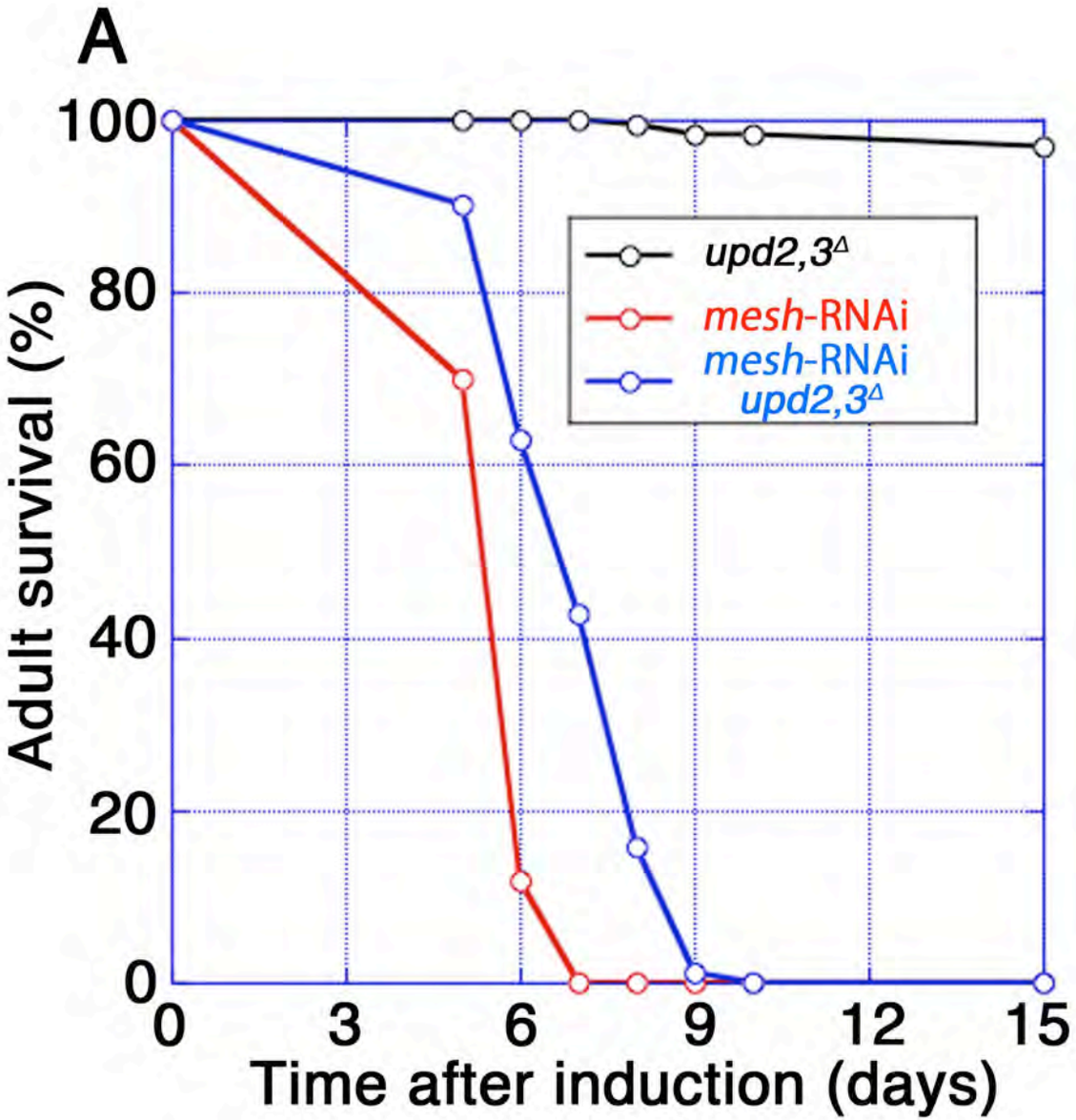

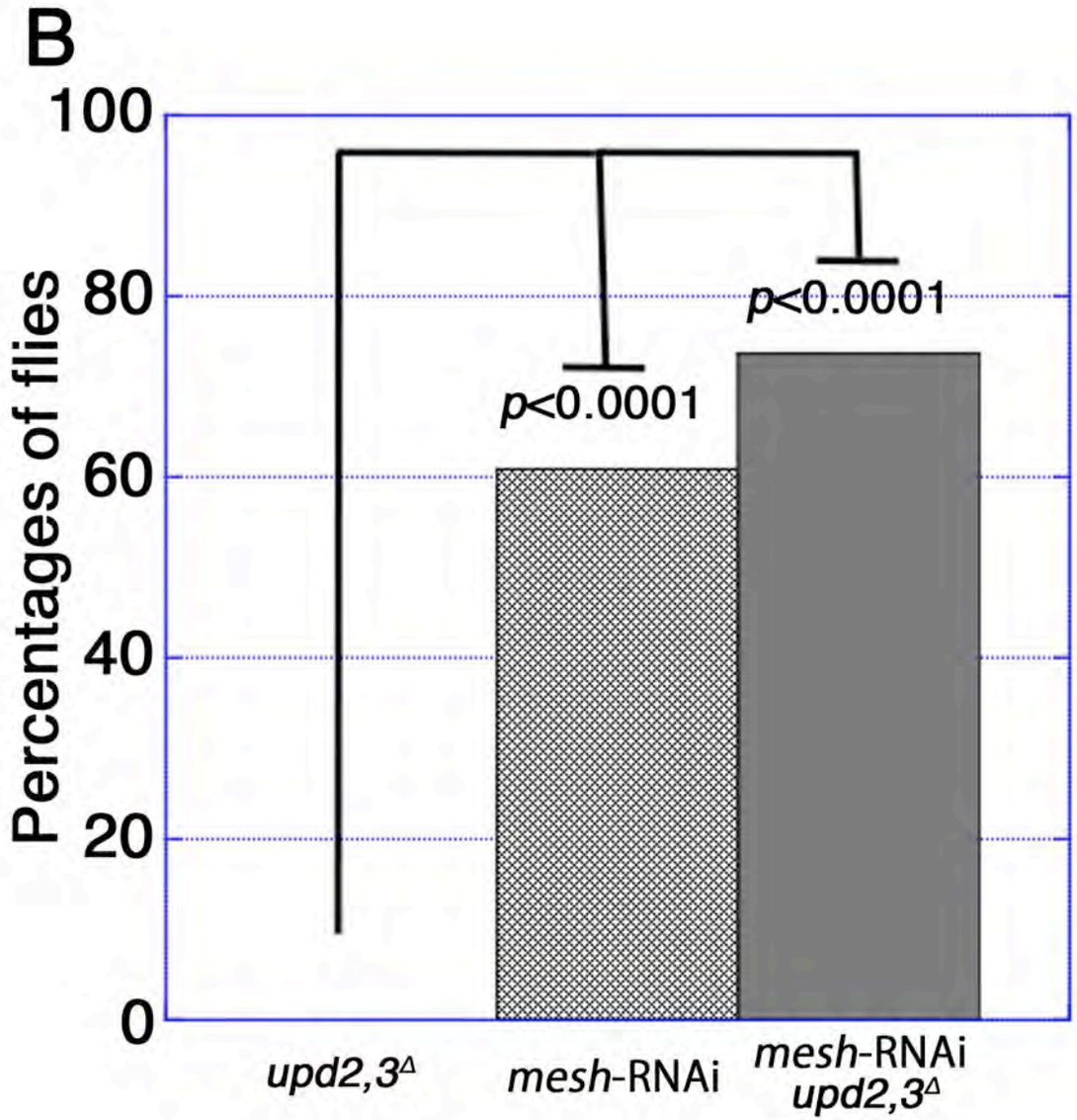

Izumi et al., Figure S7